Acta Biomaterialia 95 (2019) 91–111

Contents lists available at ScienceDirect

Acta Biomaterialia

journal homepage: www.elsevier.com/locate/actabiomat

Review article

Integration of biological systems with electronic-mechanical assemblies ☆

Ning Yi [a], Haitao Cui [b], Lijie Grace Zhang [b,c], Huanyu Cheng [a,d,*]

[a] Department of Materials Science and Engineering, The Pennsylvania State University, University Park, PA 16802, USA
[b] Department of Mechanical and Aerospace Engineering, The George Washington University, Washington, DC 20052, USA
[c] Departments of Electrical and Computer Engineering, Biomedical Engineering, and Medicine, The George Washington University, Washington DC 20052, USA
[d] Department of Engineering Science and Mechanics, and Materials Research Institute, The Pennsylvania State University, University Park, PA 16802, USA

ARTICLE INFO

Article history:
Received 1 November 2018
Received in revised form 10 April 2019
Accepted 11 April 2019
Available online 17 April 2019

Keywords:
Biological systems
Electronic-mechanical assemblies
Cell culture
Tissues and organoids
Organs and living individuals

ABSTRACT

Biological systems continuously interact with the surrounding environment because they are dynamically evolving. The interaction is achieved through mechanical, electrical, chemical, biological, thermal, optical, or a synergistic combination of these cues. To provide a fundamental understanding of the interaction, recent efforts that integrate biological systems with the electronic-mechanical assemblies create unique opportunities for simultaneous monitoring and eliciting the responses to the biological system. Recent innovations in materials, fabrication processes, and device integration approaches have created the enablers to yield bio-integrated devices to interface with the biological system, ranging from cells and tissues to organs and living individual. In this short review, we will provide a brief overview of the recent development on the integration of the biological systems with electronic-mechanical assemblies across multiple scales, with applications ranging from healthcare monitoring to therapeutic options such as drug delivery and rehabilitation therapies.

Statement of Significance

An overview of the recent progress on the integration of the biological system with both electronic and mechanical assemblies is discussed. The integration creates the unique opportunity to simultaneously monitor and elicit the responses to the biological system, which provides a fundamental understanding of the interaction between the biological system and the electronic-mechanical assemblies. Recent innovations in materials, fabrication processes, and device integration approaches have created the enablers to yield bio-integrated devices to interface with the biological system, ranging from cells and tissues to organs and living individual.

Contents

☆ Part of the Cell and Tissue Biofabrication Special Issue, edited by Professors Guohao Dai and Kaiming Ye.

* Corresponding author at: Department of Engineering Science and Mechanics, and Materials Research Institute, The Pennsylvania State University, University Park, PA 16802, USA.
E-mail address: huanyu.cheng@psu.edu (H. Cheng).

https://doi.org/10.1016/j.actbio.2019.04.032
1742-7061/

1. Introduction

The length scale of complex biological systems ranges from micrometer in cells to meter in living individuals. Because of the dynamically evolving nature, the biological system continually interacts with its surrounding environment. For instance, automatic contraction and elongation of myofibers in cardiomyocytes during the polarization and depolarization processes induce heart chambers and ventricles to mechanically deform, whereas the exposure of differentiated cardiomyocytes to cyclic strain facilitates their maturation [1]. As another example, neurons transmit action potential through the axon and synaptic connections, whereas the application of low-frequency electrical stimulation effectively promotes the axonal regeneration after surgical repair [2]. Besides mechanical and electrical stimuli, the interaction between the biological system and its surrounding environment could be achieved through chemical, biological, thermal, optical, or a synergistic combination of these cues. To provide a fundamental understanding of the interaction, recent efforts that explore the opportunity to integrate the biological system with electronic-mechanical assemblies allow sensing and actuating modules to record and elicit the responses simultaneously.

The recent advances of new materials, fabrication processes, and device integration approaches have promoted the development of biocompatible bio-integrated devices to interface with the biological system both *in vitro* and *in vivo* across multiple length scales. Leveraging the rapid progress in the microelectromechanical systems (MEMS), early efforts start to integrate the cells and tissues with miniaturized sensors and actuators, resulting in the capabilities for drug discovery and disease modeling. Most of the biological systems in this type of integration are, however, limited in size due to the lack of 3D structures and vascular networks that are ubiquitously found in most forms of life. As a versatile fabrication route, 3D printing can help create structures with the designed shape, porosity, and other properties that are not easy to obtain with the traditional fabrication processes. A variety of advanced 3D printing approaches include stereolithography [3], inkjet printing [4], fused deposition modeling [5], selective laser sintering [6], and many others. The 3D printing has also been successfully demonstrated in the biomedical applications, ranging from tissue scaffolding [7] and surgical preparation [8] to pharmaceuticals [9]. With these 3D printing approaches, complex functional tissue structures have been created, promoting the rapid development in the field of 3D bioprinting. In particular, the 3D perfused vascular network from bioprinting enables the creation of 3D tissues and even organs because of their crucial role in the efficient transport of nutrients and the promotion of tissue formation. As an alternative approach to 3D bioprinting in mechanical assembly, a class of 3D structures created from mechanically guided assembly provides opportunities that could complement the existing approaches. Based on direct 3D printing [10,11], templated growth [12,13], or many others, most of the approaches are limited by the materials that can be used or by the range of geometries that can be formed. To explore design options beyond these constraints, researchers have investigated mechanical compression-induced buckling to transform 2D micro/nanostructures into previously inaccessible classes of 3D layouts with wide-ranging materials [14–17].

The integration of biological systems with electronic-mechanical assemblies allows the assemblies to elicit and monitor the behavior of the cell at the cellular level, including attachment, differentiation, proliferation, and apoptosis. At the tissue level, the integration that resembles the natural environment enables the application of three-dimensional tissue constructs to drug screening and disease modeling. When the living individual is of concern, various other factors such as the level of comfort or the foreign body response would have to be considered. Therefore, it is highly desirable to explore deformable devices that can conform and deform to the dynamically changing surface of the soft skin or organs. Such integration provides an essential platform for healthcare monitoring and therapeutic options such as drug delivery and rehabilitation therapies. This short review will give a brief overview of the recent development on the integration of the biological systems with electronic-mechanical assemblies across multiple scales (i.e. from the cellular level to tissue/organ level and then to the living individual). We will first introduce the integration of cell and tissue culture with electronic assemblies with a focus on organ-specific tissue toward drug screening in Section 2. Section 3 will focus on the integration with mechanical assemblies enabled by the 3D bioprinting and mechanically assembled 3D structures. Next, we will review the recent efforts on the integration of explanted organs and living individuals with electronic-mechanical assemblies for health monitoring and smart drug delivery. Finally, we will conclude with the challenges and opportunities, highlighting a fraction of critical future directions in the burgeoning field of integrating biological systems with electronic-mechanical assemblies.

2. Integration of cells and organoids with electronic assemblies

In this section, we will first introduce the basic concept of cell culture and the importance of multiple cues. Next, we will discuss the integration of cell culture with electronic sensors for continuous monitoring of various signals and thus the culturing process. As a collection of organ-specific cell types developed from stem cells or organ progenitors, organoids are capable of recapitulating some specific function of the organ. Integration of organoids with electronic sensors for drug development is then discussed.

2.1. Cell culture with multiple cues

Since the early effort on the outgrowth of the nerve fiber over a century ago [18], two-dimensional (2D) cell culture grows into a mature methodology. The technique is attractive because it allows the researchers to continuously study the behavior of the cells free from the influence of the surrounding body of the organism. Though the initial effort has demonstrated an enormous impact on the biomedical research, cell culture in a static aqueous environment has been associated with several challenges, including cell waste accumulation, nutrition depletion, and its inability to

maintain differentiated functions of many cell types [19]. As a result, control in the flow of the culture medium is introduced to overcome these challenges. Capable of providing precise control over the flow rate, microfluidic devices with inlets and outlets can facilitate medium exchange and deliver growth factors [20].

Besides the growth factors, the chemical and physical properties of the extracellular matrix (ECM) also show significant impacts on the cell culture. The physical features of the ECM include stiffness, geometry, ligand spacing, and even time-dependent properties such as viscoelasticity, matrix stiffening and degradability over time, and spatial patterning [21]. Because many of the physical properties are tightly coupled with the externally applied loading, multiple cues such as tensile strain and electrical stimulation demonstrate particularly strong influence. For instance, the tensile strain can guide cellular alignment, tissue maturation, gene expression, lineage commitment, and tissue engineering of multiple mechanically functional tissues such as cardiac, muscle, vasculature, ligament, tendon, and bone [22]. Besides, targeted delivery of nanoparticles (NPs) can also be mediated by the differential mechanical states of cells that are directed by culturing cell lines (HeLa and HCT-8) on hydrogels of various stiffnesses because of mechanotransduction [23]. The *in vitro* NP delivery demonstrates that the increased cell stress suppresses its cellular uptake, dominating over the enhanced uptake from the increase in the exposed surface area from the cell spreading. In addition to mechanical cues, several studies have shown electric cue significantly affects the development of neural and cardiac tissues, mainly because of the voltage-gated calcium channels of the cell membrane. The electric cue regulates crucial physiological functions such as muscle contraction and neuronal excitability. Electrical stimulation devices that deliver electrical cues throughout the engineered tissue constructs can improve cell-cell communication and functions [24].

2.2. Integration of cell culture with electronic sensors

The absence of sufficient means to probe the cultured cells makes it difficult to track and signal the crucial steps of the culture process. Therefore, the electronic sensors that provide the sensing capabilities promote the study of cell culture. The necessary signals to monitor include chemical species [25], mechanical deformation (e.g., strain [26], liquid flow velocity and pressure [27,28]), and the electrical impedance [29]. The commonly used microfluidic devices integrated with chemical sensors provide the capability to probe the cells in real time during culture. Chemical species can be detected either through direct physical detection (electrical, optical, or mechanical indices) or from the enzyme-based reaction. As one representative example, the nitric oxide (NO) produced by endothelial cells functions as an essential mediator of multiple processes involved in the cardiovascular, nervous, and immune systems. Integrating free radical sensor on endothelialized PDMS blood vessels enables the real-time electrochemical detection of NO concentration upon drug treatment [25]. The treatment with amiodarone and acetaminophen induces the vascular endothelial cells to produce an elevated level of NO, followed by a decrease to the baseline within a few minutes, consistent with the literature [30]. The electrochemical method also allows the monitoring of the other bio-related chemical species such as lactate, glucose [31–33], and metal ions [34]. As a popular method to grow scaffold-free tissues with a spherical shape, the hanging-drop network can integrate lactate and glucose sensors to monitor the metabolism of cultured microtissue through the detection of lactate and glucose levels (Fig. 1A) [31]. By detecting glucose consumption and lactate secretion through hydrogen peroxide that is produced by glucose oxidase and lactate oxidase, the functionalized and calibrated sensor tracks the increased glycolysis metabolism of the cancerous tissue. While the lactate secretion from anaerobic glycolysis leads to an acidic extracellular pH level in the tumors [35], the insufficient supply of oxygen often causes variation of the cellular metabolism [36]. To monitor these metabolic activities, an optical method with Si photodiodes and light emitting diode (LED) is explored to provide the real-time detection of pH and dissolved oxygen levels (Fig. 1B) [37]. Upon exposure to different pH values, the absorption spectra of phenol red changes to result in a difference in the current value generated by the photodiodes. The ruthenium dye with oxygen-sensitive fluorescence embedded in PDMS changes its intensity and the resulting current in the photodiode beneath a blue LED is then correlated with the oxygen concentration [38]. The pH value reflects the acidic condition of the fluid resulted from the secreted ammonia and lactate by cells and dissolved oxygen evaluates the oxygen supply to the cells.

Mechanical signals can also be necessary. A representative example is to monitor the pressure from the flow generated by the cardiac cells of various clinically relevant physiologic conditions for replicating dysfunctional myocardium [39]. In one demonstration, when the flow passes through the channels integrated with piezoelectric poly (vinylidene fluoride) nanofibers, electrical output is generated from the deformation of the nanofibers. As the deformation is affected by the viscosity and velocity of the fluid, the deformation-induced voltage output can detect the associated properties of the fluid. Because of the piezoelectric open-circuit voltage as high as 1.8 V, the sensor can also convert the mechanical energy from the fluid to electrical energy for creating a self-powered sensing system [27].

The electrical impedance at the cell-electrode interface is affected by the electrode-medium interface, the medium, the adherent cells, and cell-cell interactions. Therefore, performing the electrical impedance spectroscopy can provide critical information on differentiation [40], adhesion [41], and proliferation [42] of the cells. With 378 channels in a self-developed microelectrode array (MEA), the differentiation process of the neural pluripotent stem cell can be tracked (Fig. 1C) [43]. Tracking of the relative impedance calculated from the cell-covered and cell-free electrodes shows a decrease over the progress of cell differentiation. The decline is attributed to the formation of the long dendrites and axons by neurons, which reduces the tight cell-cell contacts [44]. When integrated into a microfluidic device, the electrical impedance measurement is also demonstrated as a cell growth rate monitor (Fig. 1D) [45]. Upon saturation of the cell culturing area in the clamping pad, the continuous proliferation of cells prompts cells to pass through the electrodes guided by the two hexagonal structures. Correlating the change of the impedance value with the number of cells establishes the tracking. As the *trans*-epithelial electrical resistance (TEER) measures electrical resistance over a tissue barrier, the TEER can be used to quantify the barrier integrity and permeability in the endothelial cell layer [46]. Combining two TEER electrodes to assess the integrity of the endothelium with an MEA of 57 platinum electrodes to measure field potentials of cardiomyocytes, the system could simultaneously study cell barrier function and electrical activity of an endothelialized cardiac model (Fig. 1E). The growth of the endothelium increases the impedance value between two TEER electrodes and the decreased slope of impedance over time indicates the proliferation of cells. Capable of detecting the inflammatory stimulus tumor necrosis factor alpha (TNF-α) or the cardiac targeting drug isoproterenol, the system provides a platform for the real-time assessment of biological functions and response to therapeutics.

2.3. Integration of organoids with electronic sensors for drug screening

Organoids integrated with multiple sensors yield a platform for the study of tissue function and disease modeling [47,48], but more

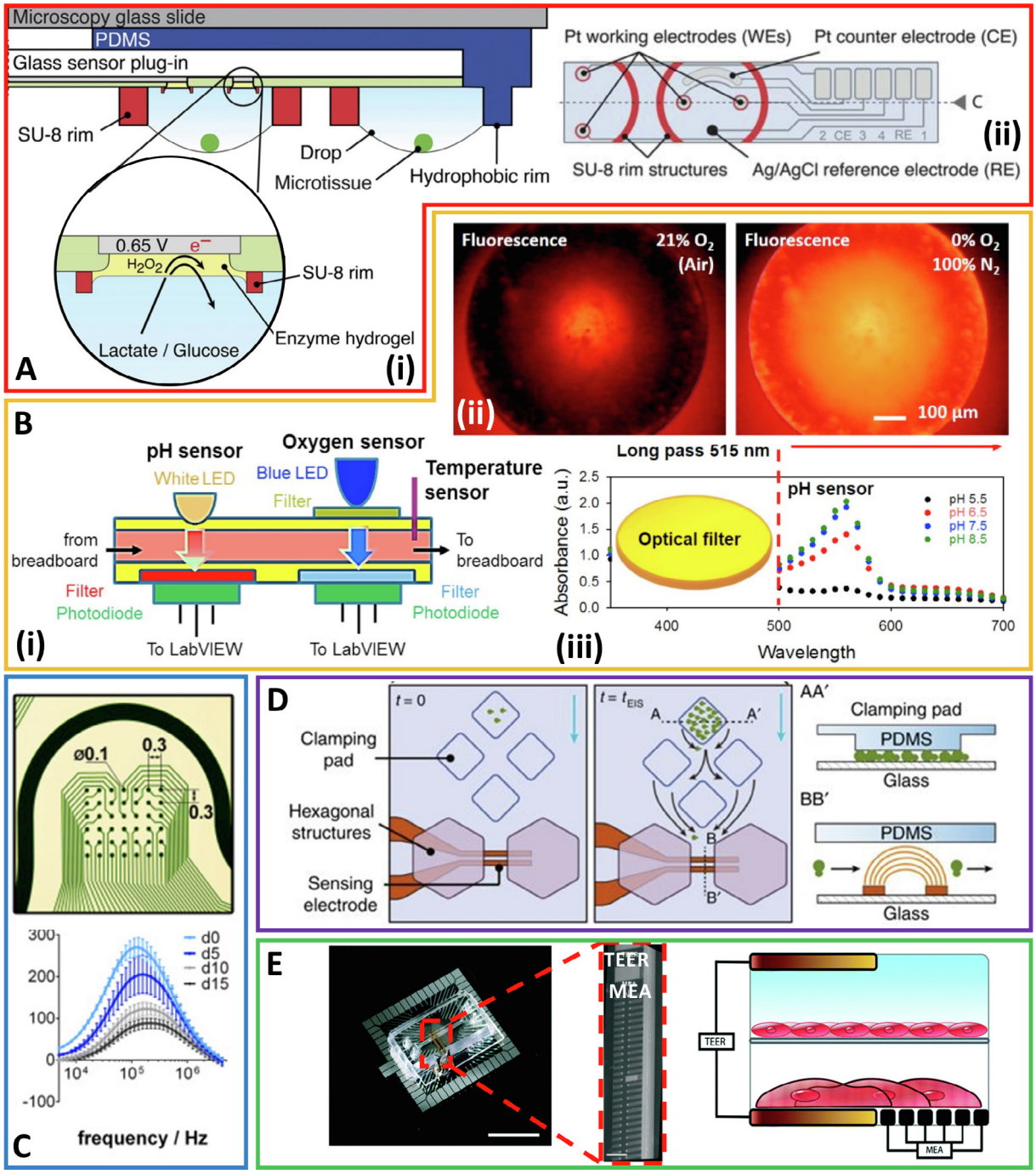

Fig. 1. (A) (i) Cross-sectional schematic diagram of the hanging-drop network showing the multilayer structure with a close view of the lactate/glucose sensor. (ii) Top view of the sensing unit built on a glass slide with four working electrodes, one counter electrode, and one reference electrode. Reproduced with permission from [33]. (B) (i) Cross-sectional schematic diagram of the pH, oxygen, and temperature sensing elements incorporated into the platform. (ii) Photo images showing the fluorescence intensity of the ruthenium dye embedded in PDMS under different oxygen concentration. (iii) Absorption spectra of phenol red pH sensor under different pH levels. Reproduced with permission from [40]. (C) The configuration of electrodes on the microelectrode array (MEA) and the measured impedance shifts to a smaller value as neural cells proliferate. Reproduced with permission from [45]. (D) Top view of the cell growth rate monitor composed of clamping pad, hexagonal support structures, and sensing electrodes. Blue arrows indicate the media flow direction and black arrows indicate the trajectories of the cells escaped from the clamping pad. The inset on the right provides cross-sectional views of the AA' plane and BB' plane showing the growth of cells at the clamping pad and passage of the cells through electrodes. Reproduced with permission from [47]. (E) Picture of the TEER electrodes and MEA integrated into a microfluidic chip. Scale bar: 2 cm. The exploded view shows the SEM images of the TEER electrodes and MEA. Scale bar: 500 µm. The inset on the right shows the side view of the microfluidic chamber with cultured endothelial cells and cardiomyocytes on both sides of the thin PET membrane sandwiched by the TEER electrode and MEA. Reproduced with permission from [48]. (For interpretation of the references to color in this figure legend, the reader is referred to the web version of this article.)

importantly for drug screening as extensively discussed in a recent review article [49]. As pharmacokinetics strongly depends on the morphology and physiology of various tissues and organs, the microfluidic devices with functional units of different organoids bear great importance for drug screening. The small dimension of microfluidic chambers and channels reduces sample consumption and facilitates heat transfer and mass transport [50]. The significant interest in drug test [51] has spurred rapid development of various organoids, including heart [52], lung [53], brain [54], kidney [55], liver [56], gut [57], bone marrow [58], muscle [59], and

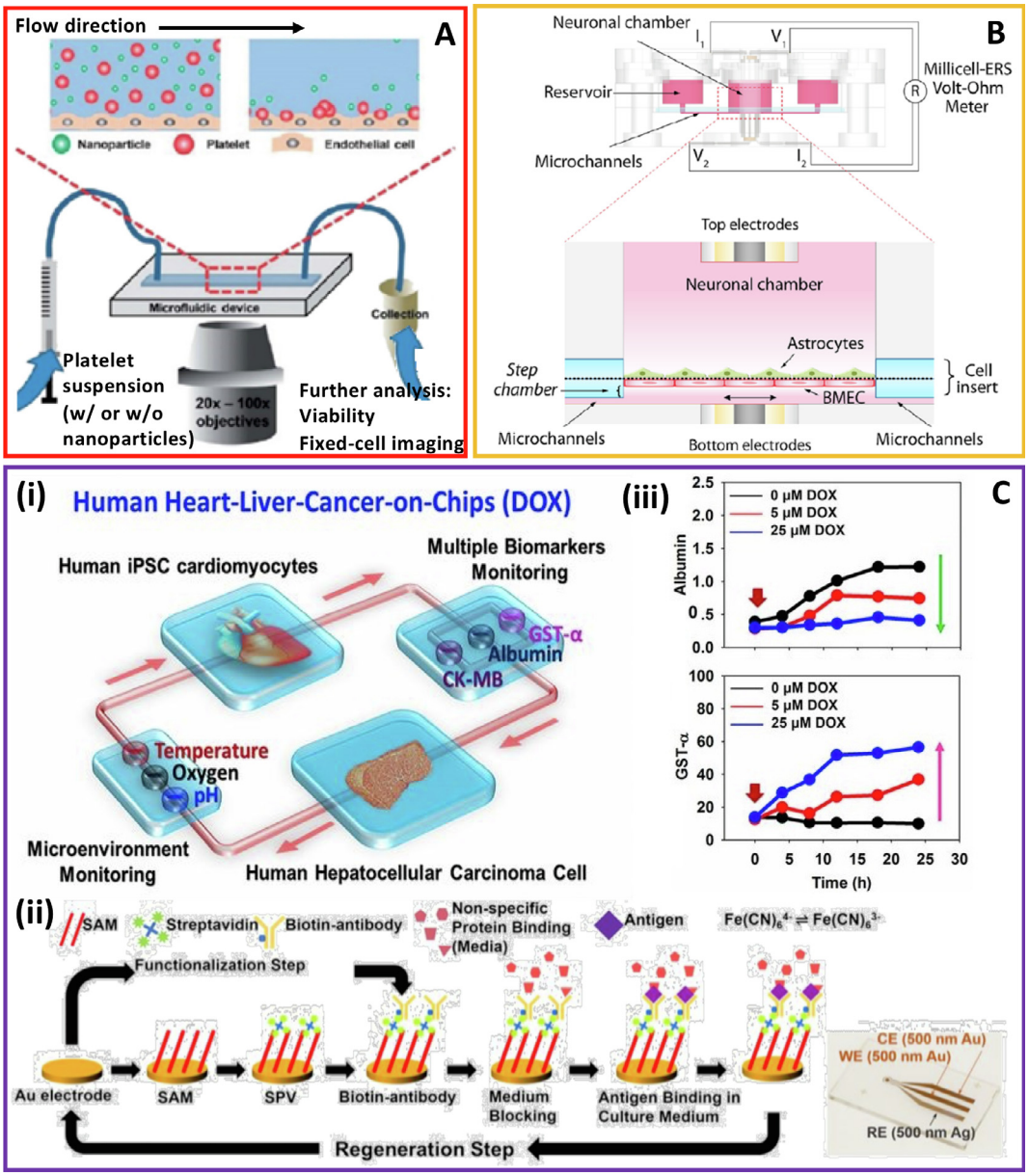

Fig. 2. (A) Microfluidic device with microscope integrated to observe the platelet-endothelial adhesion and platelet aggregation. Reproduced with permission [67]. (B) A cross-sectional view of the TEER electrode integrated BBB on-chip model for evaluation of vascular toxicity of DOX. BBB: blood-brain barrier. Reproduced with permission [69]. (C) (i) Schematic diagram of biomimetic human heart-liver-cancer tissues-on-chip that is composed of two culturing chambers, microenvironment monitor platform, and biomarkers detection module. (ii) The functionalization and regeneration process of the electrode for soluble antigens measurement. (iii) Real-time automated measurements of albumin and GST-α secreted from the human hepatocellular carcinoma cells. Reproduced with permission [40].

blood vessels [60], commonly termed as organ-on-a-chip. It should be pointed out that the creation of certain organoids would need external cues. For instance, the cyclic strain that mimics peristaltic motions of intestinal is used to create a gut-on-a-chip model [57], which has also been applied to create a lung-on-a-chip model [61]. Connecting multiple chambers with different organoids cultured inside results in a more complicated system to model drug transport from the vascular system to different organs [62].

In comparison to chemiluminescence, surface plasmon resonance, mass spectrometry, and electrochemical absorption [50], fluorescence analysis such as fluorescent stains and immunofluorescence is by far the most popular approach for the real-time monitoring of cultured organoids [63] due to its high-sensitivity. The adhesion and aggregation of platelet can be directly observed on a blood vessel-on-a-chip upon exposure to mesoporous silica nanoparticles (Fig. 2A) [64]. Even though capable of characterizing cell activities in organoids, most fluorescence-based methods require the staining process, leading to frequent interruption of the culturing process and a large working volume. Also, the reactive oxygen species produced by fluorophores poses concern of phototoxicity in the living cells [65]. Therefore, it is of great interest to integrate organoids with electronic sensors for drug screening. The drug permeability screening is conducted by combining a blood-brain barrier (BBB) on-a-chip model with a TEER electrode (Fig. 2B) [66]. After applying doxorubicin (DOX), an antineoplastic agent that is widely used for cancer treatment, the measured TEER value decreases significantly. The decrease in the TEER value implies the compromised integrity of the cultured BBB due to the vascular toxicity of doxorubicin.

Integrating the organoid with electrochemical electrodes also allows detection of biomarkers secreted by the organoids. One representative example is to use the human heart-liver-cancer-on-

Table 1
Electronic sensors integrated with organoids for drug screening.

Analyte	Limit of detection/ sensitivity	Detection method	Organoid type	Drug	Refs.
NO	140 nM	Free radical	Human endothelial cells	Amiodarone, Acetaminophen	[25]
Lactate & glucose	0.5 mM	Amperometric	Human liver cancer cells	Acetaminophen, Amiodarone, Troglitazone, Rotenone	[32]
Potassium ion	$10^{-3.18\pm0.03}$ mM	Potentiometric	Human liver cancer cells	Acetaminophen	[34]
pH	0.03 pH	Potentiometric	Human dermal fibroblasts	–	[37]
Oxygen	$-0.735\ \mu A\mu M^{-1}cm^{-2}$ $-7mV/O_2\%$	Amperometric Photodiode	Human glioblastoma cells Human primary hepatocytes Human cardiac organoids	Cytochalasin B Doxorubicin Acetaminophen	[67,38]
TEER	–	Impedance spectroscopy	Brain microvascular endothelial cells	Fluorescein isothiocyanate dextran, Cimetidine, Doxorubicin	[66]

chips platform to examine the effect of DOX on treating liver cancer (Fig. 2C, i) [38]. Based on the change of interfacial electron transfer kinetics of a redox probe upon antibody-antigen binding events, the electrode surface functionalized with specific antibodies can detect the binding biomarker. As the biomarker captured on the electrode surface would saturate after a few binding events, a dual-cleaning process is used to regenerate the electrode surface upon saturation of the captured antigen. The cleaning process relies on the use of a self-assembled monolayer (SAM), which enables the easy removal of antibody/antigen complexes by breaking the thiol-Au bond with an electrochemical method (Fig. 2C, ii). When multiplexed, the immunobiosensor chip can measure multiple biomarkers such as liver biomarkers albumin, glutathione S-transferase α (GST-α), and cardiac biomarker creatine kinase MB (CK-MB). The increase of DOX dose from 0 to 25 μM causes increased GST-α secretion and diminished albumin secretion, indicating the death of liver cancer cells (Fig. 2C, iii). Capable of detecting soluble biomarkers *in situ* without manual interference, the automated platform can study the dynamics of drug effects over extended periods (See Table 1).

3. Integration of tissue constructs with electronic-mechanical assemblies

In this section, we will first introduce bioprinted structures as mechanical assemblies for 3D cell/tissue culture. Because it is of significant interest to integrate tissue constructs with electronic-mechanical assemblies, we will further discuss the integration of bioprinted tissue constructs with electronic sensors. Forming the complex 3D structures with the advanced materials creates additional opportunities in the field of tissue scaffolds, because the use of advanced materials allows easy integration of multifunctional sensing and actuating modules into the tissue scaffolds. Next, we will review the relevant design concepts to create mechanical assemblies from the mechanically guided assembly process. The discussion of the typical application in tissue scaffolds with integrated sensing modules will then be used to illustrate the integration with electronic-mechanical assemblies.

3.1. Mechanical assemblies from bioprinted structures

To overcome the limitations of 2D cell culture, researchers have developed 3D cell culture models with the use of hydrogels [68], synthetic polymers [69], and extracellular matrix (ECM) molecules [70] to provide a better cellular microenvironment for the *in vitro* studies. The generated complex 3D structures in culture can closely parallel their *in vivo* counterparts. Moreover, multiple cues can be readily integrated into the complex 3D structures from bioprinting. Compared with the flow-induced permeation commonly used in 2D cell culture, perfusable culture can be more beneficial for ensuring homogenous and efficient mass transport, especially with vascularization. The vascularized tissue constructs have been developed by integrating perfusable vessel channels and capillary-like networks (Fig. 3A) [71,72]. The representative hydrodynamic parameters of permeability (K_D) and average shear stress (τ) can be controlled within the range of venous shear stress noted in microcirculation. It is demonstrated that fluidic cues can improve vasculogenesis or angiogenesis by mimicking the shear stress and providing a hypoxic environment through gradient oxygen diffusion. Moreover, shear forces created by medium flow through the tissue scaffolds can mimic hemodynamic forces and pressures that occur naturally in the human body thus improving extracellular matrix (ECM) production and mechanical properties of the artificial tissues/organs [73].

The electric cues that are important for muscle contraction and neuronal excitability can be easily achieved through the use of conductive materials [74], including conductive polymers, multi-walled carbon nanotubes, and carbon nanofibers, among others. By integrating the conductive scaffold with biphasic electrical stimulation, neural stem cell proliferation on carbon fiber scaffolds is promoted [75]. The upregulated neuronal gene expression levels and increased microtubule-associated protein 2 immunofluorescences demonstrate an improved neuronal differentiation and maturation. Though adipose-derived stem cells (ADSCs) have the capacity to differentiate into neural precursor cells, further clinical applications are limited by their inherently low neurogenic differentiation efficiency. After neurogenic differentiation with electrical stimulation, the ADSC aggregates in conductive microwells express greater positive neuronal differentiation markers compared to non-stimulated microwells [76]. This result indicates that electrical stimulation of cell aggregates in conductive microwells is an effective method for increasing neurogenic differentiation.

As an advanced and emerging technique, 4D bioprinting offers excellent potential for fabricating complex, stimuli-responsive 3D biological structures. The 4D process may elicit proper biological responses that not only mimic the dynamic growth process of native tissues/organs, but also achieve a more complicated, dynamic architecture for tissue implants that meet the criteria of multiple variations with precisely controlled stimuli processes [77]. By incorporating shape transformation within material/structural design, the printed objects can self-transform in form or function via mechanically induced reassembly when exposed to a predetermined stimulus, including osmotic pressure, solvent, pH, exposure to heat, current, light, or other energy sources [77–79]. Typically, the shape transformation or reprogramming design can be achieved by leveraging the anisotropic properties of the material (through aligned printing or varying the crosslinking density) or by depositing multiple inks with distinct features. 3D network structures have been printed with heterologous droplets in software-defined arrangements to replicate the sophisticated collective behavior from cells to tissues (Fig. 3B) [80,81]. The bilayers

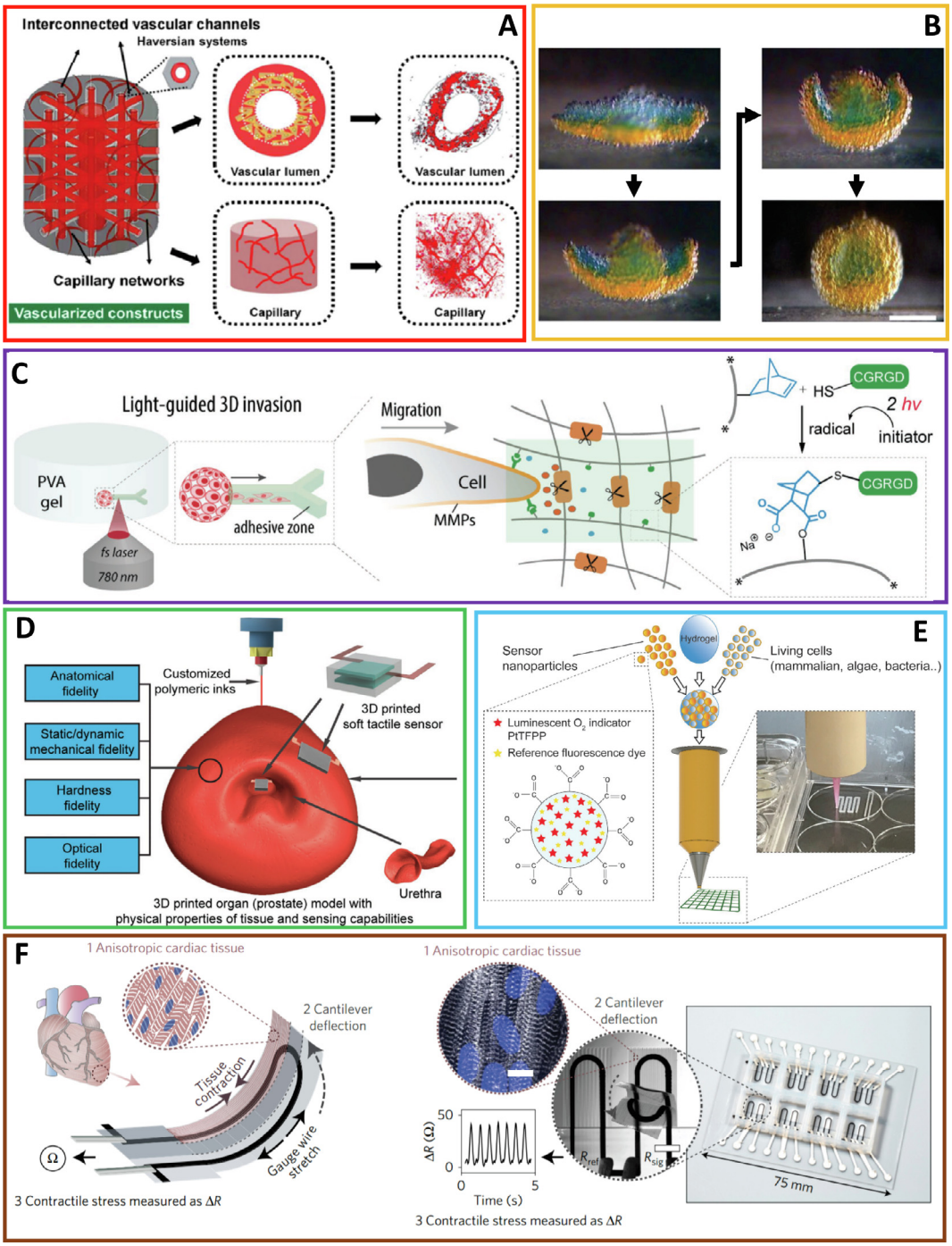

Fig. 3. (A) Schematic illustration of a vascular structure constructed based on matrix metalloprotease (MMP) sensitive hydrogel. The formation of the vascular lumen and capillary network can be achieved during culture. Reproduced with permission [73]. (B) Photographs of flower-like droplet networks that can self-fold into a hollow sphere in 8 h. Orange and blue droplets contain KCl with different concentrations (blue: 8 mM orange: 80 mM). Scale bar: 200 μm. Reproduced with permission [82]. (C) Schematic of light-guided 3D invasion within polyvinyl alcohol (PVA) gel with cell-instructive extracellular cues attached to the PVA matrix site-specifically through the thiol-ene conjugation. Reproduced with permission [84]. (D) A patient-specific prostate model reconstructed by 3D printing with tissue properties and sensing capability (provided by a 3D printed soft tactile sensor) for advanced surgical rehearsal. Reproduced with permission [88]. (E) Formulation of the bioink mixed with living cells and nanoparticles that contain oxygen-sensitive luminescent indicator and reference fluorescence dye. Reproduced with permission [89]. (F) Schematic illustration of a 3D printed anisotropic cardiac tissue bending a cantilever to induce stretching in the integrated soft strain gauge (left) and its corresponding photograph (right). Periodic contraction of the cardiac tissue can be tracked by the change of resistance value of the strain gauge. Reproduced with permission [90]. (For interpretation of the references to color in this figure legend, the reader is referred to the web version of this article.)

of lipid-coated aqueous droplets allow the compartments to interact directly through membrane proteins or osmotic flows of water. The interaction enables the engineering of collective properties in the printed droplet network such as long-range electrical communication or macroscopic deformation [81]. Printed droplet networks could potentially interface with tissues either as tissue engineering substrates or as mimics of tissues.

As an alternative to explore the anisotropic properties, responsive materials are also widely used for the shape transformation. Through the use of cell-responsive hydrogel composed of

peptide-crosslinked polyvinyl alcohol (PVA), focusing an ultrafast multiphoton laser into the cell-laden PVA hydrogel allows the attachment of cell-instructive extracellular cues to the PVA matrix, precisely guiding the cell invasion in 3D (Fig. 3C) [82]. Moreover, shape memory and self-healing polymers are attracting more attention in 4D printing due to their unique "stimuli-responsive" physical characteristics [77]. Soybean oil epoxidized acrylate inks have been printed by stereolithography (SL) system for creating the smart and highly biocompatible scaffolds capable of supporting the growth of multipotent human bone marrow mesenchymal stem cells (hBMSCs) [83–85]. Photolithographic-stereolitho graphic-tandem strategy (PSTS) refers to the sequential treatment of the ink feedstock with photolithography and stereolithography. The tissue scaffolds fabricated with a PSTS process not only possess subtle surface micropatterns but also exhibit dynamic 4D shape change after external stimulation [83]. A 4D reprogrammable nerve guidance conduit has been demonstrated with hBMSCs that high-potentially differentiate into aligned neural cells on the SL-induced surficial microstructures [84]. The unique graded internal stress followed by a solvent-induced relaxation drives a reversible change of the programmed configuration. Additionally, the shape memory construct can trigger a "thermomechanical programming" shape transformation, thereby achieving a multiple-responsive 4D effect. The 4D printing technique provides dynamic tissue scaffolds with proper physical guidance and chemical cues, seamlessly integrated in a minimal invasion manner.

3.2. Integration of bioprinted tissue constructs with electronic sensors

Integrating bioprinted tissue constructs with relevant sensors enables the evaluation of the bioprinted tissue. Though the structure of the patient's organ reconstructed from the traditional 3D printing method can show the anatomies and disease states of the organ toward pre-surgery models, it doesn't have the similar mechanical, optical, and dynamic behavior of the organ. The lack of sensing elements in the structure further makes it impossible to track the force and deformation, limiting its application as a pre-operative practice tool. In an attempt to address these challenges, a prostate model is inkjet printed with a customized ink that has the same mechanical and optical properties of the prostate, integrated with a 3D printed capacitance based tactile sensor (Fig. 3D) [86]. Capable of monitoring the pressured applied with the surgical tool, the 3D printed organ model could help reduce the surgical risk by serving as a proper preoperative planning and rehearsal tool. Besides the mechanical sensor, optical sensing is demonstrated in the 3D bioprinted tissues, where luminescent optical sensing nanoparticles are added to the hydrogel bio-ink to reflect the cell metabolism by monitoring the oxygen concentration (Fig. 3E) [87]. The bio-ink is obtained by mixing cells with O_2-sensitive nanoparticles containing the platinum(II) meso(2,3,4,5,6-pentafluoro) phenyl porphyrin (PtTFPP) and an inert fluorescent dye (Bu3Coum) in an alginate/methylcellulose hydrogel. While Bu3Coum has a constant emission of green light upon excitation of blue light, PtTFPP emits red light with intensity dependent on the oxygen concentration, enabling ratiometric imaging of O_2 distributions. Compared to the hydrogel layer with nanoparticles only, the hydrogel scaffolds with microalgae and O_2 sensor nanoparticles clearly shows a spatiotemporal change in O_2 concentration, and the lowest O_2 level occurs in the hydrogel with respiring microalgae.

In direct contrast to the conventional approaches that rely on multi-step lithographic processes to create organ-specific tissues-on-chips, direct ink writing represents an attractive alternative to fabricate a new class of instrumented cardiac micro-physiological devices comprising anisotropic cardiac tissue, a structural cantilever, and a strain gauge (Fig. 3F) [88]. Multimaterial printing enables the layer-by-layer construction of dextran for the sacrificial release layer, ultrathin flexible thermoplastic polyurethane for the base layer, conductive carbon black nanoparticles for the strain sensing element, and PDMS for the surface microstructure layer that is the key for the self-alignment of the cultured cardiac tissue. Capable of tracking the development of physio-mimetic laminar cardiac tissues, the resulting device is applied to study drug responses and the contractile development of laminar cardiac tissues based on human stem cell over 28 days.

3.3. Mechanically assembled 3D structures as tissue scaffolds

The 3D assembly process relies on large compressive forces generated from the mechanical relaxation in the elastomeric substrate to lift the patterned 2D thin ribbons selectively bonded to the substrate [14]. As for the assembled 3D structures that depend on the pattern of the 2D precursor, the location of bonding pads, the level of initial pre-stretch, the mode of stretching (i.e. uniaxial vs. biaxial) [14], or distribution of the substrate thickness [89], finite element analysis guided by analytic model [90,91] has been widely adopted in the design for solving the inverse problem. The geometric transformation from 2D ribbons to 3D structures cannot be directly applied to the 2D membranes due to failure from "kink-induced" stress concentration. To address the challenge, the ideas from the art of Kirigami lead to the use of strategically patterned cuts on the 2D membranes [92]. Compared to Kirigami, the realization of origami assembly of 3D structures is associated with the challenge of the creation of the creases at desired locations. This challenge has been overcome by the spatial variation of the thickness or width to localize the deformation due to the change in bending stiffness [93] or material softening from plastic yielding [94]. The ideas of Kirigami and origami applied to the single-layer 2D precursor would lead to a buckled 3D structure with hollow interior regions. By the use of the transfer printing technique [57,95–97], multiple 2D precursors fabricated individually can be transferred and stacked to form multilayered 2D precursors, yielding nested 3D layouts [98]. Though the elastomeric substrate is an essential component of the assembly process, it also imposes engineering constraints on the realization of the freestanding 3D structures on the desired substrate. To remove such restraint, a physical transfer process that utilizes interfacial polymerization has been introduced to yield fully or partially freestanding 3D mesostructures that can be easily integrated with nearly any class of substrates [12]. The key idea to create freestanding 3D mesostructures involves the casting and curing a layer of photo-definable epoxy (SU8) with back-side exposure to define a patterned base right at the interface of the 3D mesostructured and the substrate. Immersion in HCl releases the 3D structure, and transfer printing further delivers it onto the target substrate.

As complex 3D organizations of materials are commonly found in the most sophisticated life-sustaining structures, it represents a natural yet significant interest to integrate soft biological elements with the 3D structures. Biocompatible polymer hydrogels are first applied by direct ink writing onto the 2D frameworks on the pre-strained substrate to promote cellular and tissue-level cultures, followed by the release of the pre-strain and curing of the hydrogels into place (Fig. 4A) [99]. The created 3D microscale cellular frameworks are suitable for the study of cellular migration behaviors, temporal dependencies of their growth, and contact guidance cues provided by the nonplanarity of these frameworks. While the 3D microscale cellular frameworks do not directly replicate the natural extracellular matrices, their open frameworks and out-of-plane scaffold organizations provide an addition to the material structures that can guide the tissue-level cellular organization. The culture of living cells from a model murine cell line (NIH 3T3) shows directed integration, where migration, alignment,

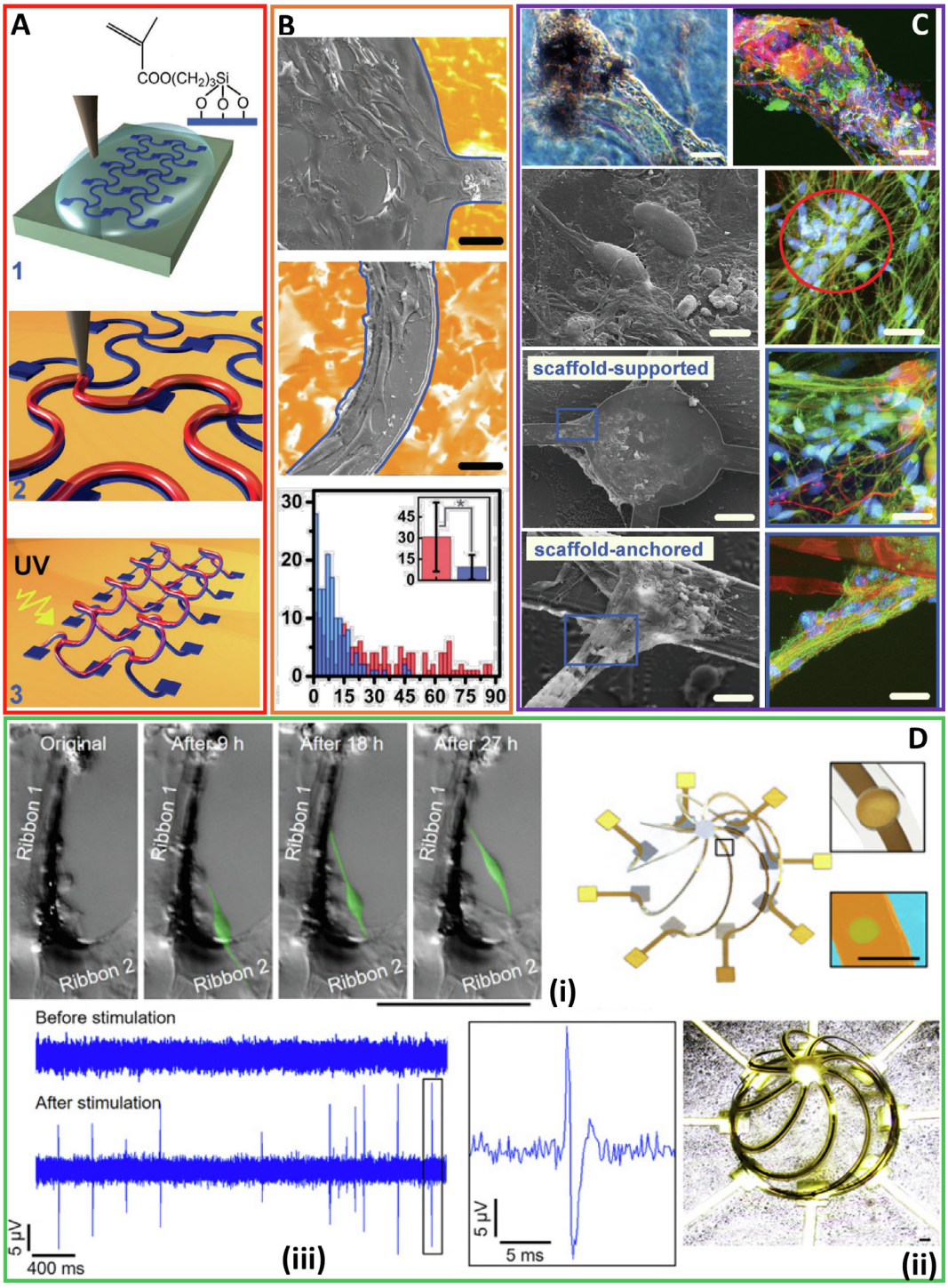

Fig. 4. (A) Schematic of the process to integrate hydrogels onto compressively buckled silicon microscale cellular frameworks: (1) silyl methacrylate surface treatment; (2) methacrylate-based hydrogel pre-polymer printing onto 2D microscale cellular frameworks on pre-strained elastomers; (3) UV treatment and release of the pre-strain buckles up the printed hydrogel into 3D structure. (B) (i) Fibroblasts with its long cell axe orient stochastically on the planar table surface, indicating the low alignment guidance leads to disordered networks. (ii) Fibroblasts with its long cell axes orient along the complex spatial vectors of the ribbon surface, indicating the high alignment guidance leads to an ordered network. (C) 1st row: mini-DRG clusters reorganized around high-aspect ratio scaffold in phase contrast (left) and immunocytochemically stained (right) mode. DRGs: dorsal root ganglia. Scale bar: 100 μm. 2nd row: Cellular sheath around DRG neurons on the table scaffold planes. Micrograph of exposed neurons (left) and a fluorescence micrograph of satellite glial cells (red circle) covering the neuron bodies (right). Scale bars (8, 20 μm). High tension fibers bridging the adjacent geometries in (3rd row) scaffold-supported and (4th row) scaffold-anchored morphologies in SEM images (left) and fluorescence micrographs. The fibers bridging adjacent table legs can be differentiated into glial, neuronal, and nuclear components as shown by the immunocytochemically staining (right) (scale bars top: 150, 15 μm; bottom: 20 μm). (A–C): Reproduced with permission from [106]. (D) (i) Observation of a DRG cell migration on a 3D ribbon *in situ*. (ii) Schematic and optical image of a 3D cage integrated with eight separately addressable electrodes for stimulation and recording. The insets show the schematic and SEM image of a representative electrode. (iii) Recording of DRG neurons collected from one 3D electrode before and after extracellular action potential stimulation with a magnified view of one spike shown on the right. (Scale bars, 100 μm). Reproduced with permission from [12]. (For interpretation of the references to color in this figure legend, the reader is referred to the web version of this article.)

Table 2
Comparison of mechanical assemblies.

Assembling method	Fabrication method	Features
Bioprinting	3D printing	Rapid prototyping, precise control of architecture, facilitated mass transport for cell culture application
	4D printing	Stimulus-responsive structure, shape transformation, capable of providing physical cues for cell culturing
Mechanically guided assembly	Patterned ribbon with origami	Controlled geometry through the level of initial pre-stretch
	Patterned membrane with Kirigami	Capable of generating hollowed 3D structure, advanced materials can be integrated onto 2D precursor before turning into a 3D structure
	Freestanding structures with transfer printing	Capable of producing a free-standing 3D structure, the assembled structure can be transferred to the target substrate of interest

and interconnection of fibroblasts occur in a time sequence over 21 days. As cell traction forces at the cell/scaffold interface regulate cell shape and propel cellular migration, the edges of the microscale cellular frameworks provide contact guidance cues to induce cellular extension and alignment adjacent to them. For instance, cells are aligned along the curvature when cultured on a solenoid ribbon (i.e., high alignment environment), whereas the long cell axes orient stochastically on a flat tabletop scaffold (i.e., low alignment environment) (Fig. 4B). As an example for tissue-level cellular structure integration, dorsal root ganglia (DRGs) isolated from rats cultured show three 3D-specific morphologies due to the scaffold's contact guidance cues and the tensile strain within the cell populations (Fig. 4C): 1) ganglion-mimetic on-ribbon clusters; 2) scaffold-supported or scaffold-anchored high tension fibers; and 3) cellular sheaths on the flat plane.

The 3D tissue scaffolds can also be created on any target substrate of interest by the use of freestanding 3D structures. In one demonstration, wax encapsulation is first applied to confine the assembled 3D structures after release from the assembly elastomer. Transfer printing the wax-encapsulated 3D structures onto a target substrate coated with an adhesive layer, followed by dissolving the wax, completes the process. Transferred 3D frameworks can serve as cellular scaffolds for guided growth of biological systems, where high-performance components such as various electronic and optoelectronic devices formed in the 2D planar design would allow interaction and communication with live cells and tissues in the assembled 3D structures. As one representative example, DRG cells can organize into networks on a bilayer 3D nested cage to either follow the 3D geometries of the scaffolds or form "shortcuts" between ribbons after cell culture of 35 days (Fig. 4D, i). Integration of an array of eight individually addressable electrodes on the 3D constructs (Fig. 4D, ii) further provides an effective means for noninvasive extracellular stimulation and recording of action potentials (Fig. 4D, iii) (See Table 2).

4. Integration of explanted organs and living individuals with electronic-mechanical assemblies

In this section, we will discuss the bio-integrated devices designed to address the mismatch in Young's modulus and shape in between the device and the skin/organ. Their applications range from diagnostic monitoring to smart drug delivery. When it comes to the application to the human body, the bio-integrated devices can be broadly classified into epidermal electronics and implantable devices. The design considerations for the former involve the level of comfort and biocompatibility, while those for the latter need to address the foreign body response specifically. The level of comfort is enabled by providing bio-integrated devices with skin-like properties. As the foreign body response may impact the biocompatibility of the bio-integrated devices, we will discuss these topics by the end of this section. Considering the extensive yet active research in this area, we will only discuss selected highlights relevant to bio-integrated devices.

4.1. Bio-integrated devices for diagnostic monitoring

The soft and dynamically changing curvilinear surface of human skin requires a conformal and tight contact of electronic-mechanical assemblies for the accurate measurement. Recent advances in stretchable skin-like devices provide application opportunities ranging from healthcare monitoring and human-machine interface to therapeutic platforms such as smart prostheses and closed-loop transdermal drug delivery. Stretchable materials and structures have been developed to enable the fabrication of the bio-integrated devices for the high-fidelity measurement of various physiological signals. The sensing modules can measure electrical (e.g., electrophysiological signals such as electrocardiogram [100], electromyogram [101], and electroencephalogram [102]), thermal (e.g., temperature and thermal transport [103,104]), mechanical (e.g., modulus and viscoelasticity [105,106]), and chemical signals (e.g., sweat characterization [107,108], blood glucose level [109], metal ion concentration [110], hydration [111]). It is worth pointing out that the signal can be coupled with different processing units for analysis. Take the analysis of chemical species in the sweat as an example, both colorimetric [107] and electrochemical [112] methods have been demonstrated to inform the health condition. The colorimetric method features easy identification of various analytes through the change of colors in the soft microfluidic patch (Fig. 5A) [107]. When it is desirable to determine the concentration of analytes precisely, the electrochemical method used in the smart wristband demonstrates the utility (Fig. 5B) [108]. Integrating the sensors with front-end circuits and wireless communication modules would further allow reading of the potassium, sodium ions, glucose, and lactate levels from sweat by a smartphone.

Besides the bio-integrated devices applied on the skin, the biodegradable devices that can fully resorb in the human body start to gain momentum, because they obviate the need for removal upon completion of the functional operation of the device [113,114]. In comparison to the devices that are designed to last, the biodegradable components and systems need to be constructed with a realistic set of biodegradable functional materials. Though biodegradable organic materials can be engineered to possess multifunctional properties as discussed in several review articles [115–117], they are often associated with compromised electrical performance. The high-performance biodegradable device based on inorganic materials [118–121] involves the use of biodegradable metals (e.g., Mg, Zn, Mo, W, and etc. [122,123]), semiconducting (e.g., Si [113], Ge, SiGe [124], ZnO [125], and etc. [126]), dielectric (e.g., Si_3N_4 and SiO_2 [127]), and insulating (e.g., biodegradable polymers [128,129] such as silk [130], gelatin [131], sodium carboxymethylcellulose [132], and galactomannan [133]) materials. By using the stretchable materials and structures [134,135], biodegradable devices components could be configured in a stretchable layout [136]. Because the use of the device grade semiconducting and conducting materials, biodegradable active and passive components can be easily demonstrated and integrated into systems. With its performance comparable to conventional counterparts, the demonstrated system provides a promising diagnostic and therapeutic platform toward implantable biomedicine. Multiplexing arrays of biodegradable silicon electrodes in either passively or actively addressed formats allows the recording of

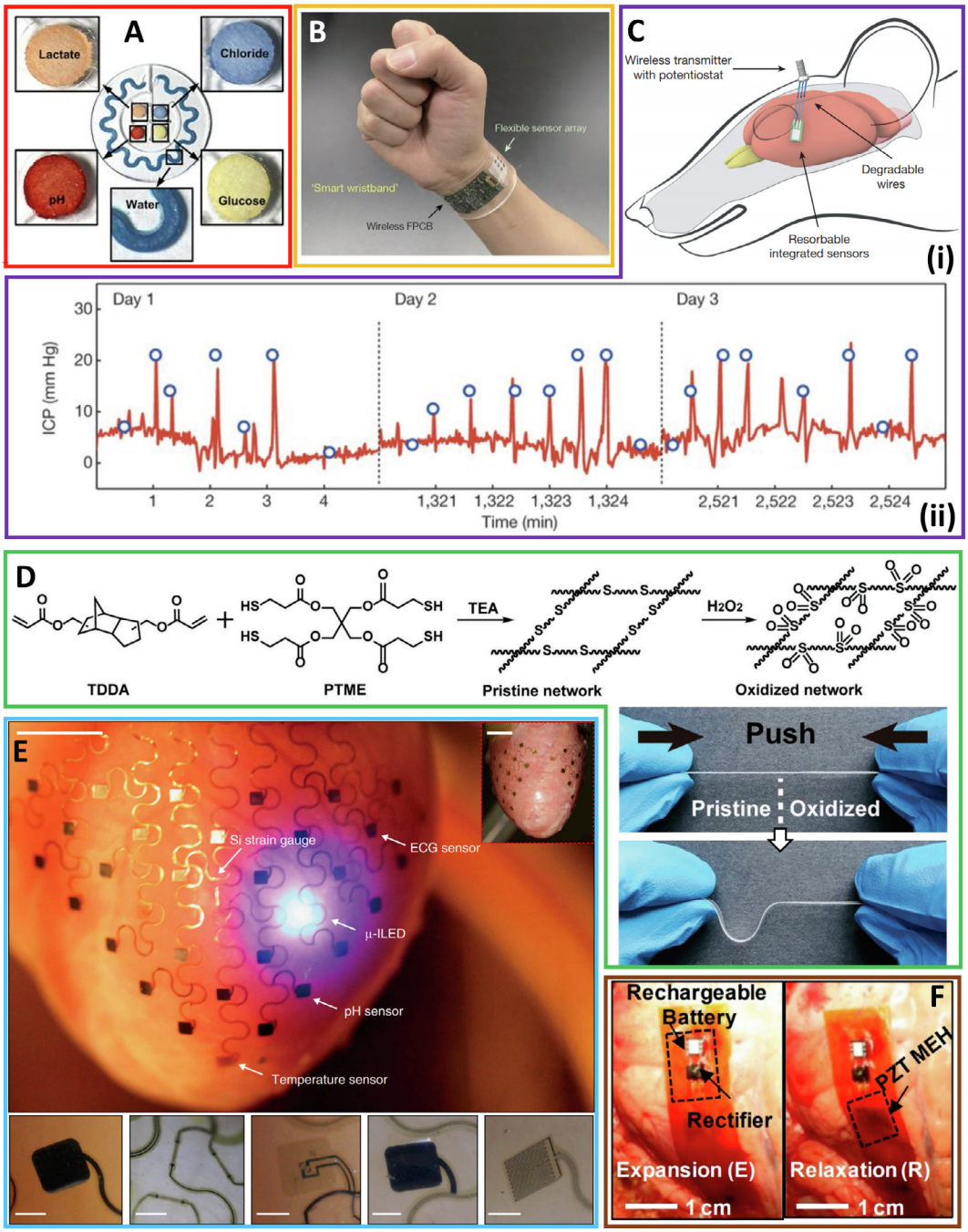

Fig. 5. Sweat sensors based on the colorimetric and electrochemical methods. (A) Dissolved analysts in sweat can cause a change of color in each chamber, which can be analyzed by the smartphone. Reproduced with permission from [115]. (B) Enzyme-based sensors integrated into a smart band can output electric current for quantifying the concentration of analysts and feed data to smartphones. Reproduced with permission from [116]. (C) (i) Diagram of a bioresorbable sensing system with pressure and temperature sensors in the intracranial space of a rat. Electrical interconnects to an external wireless data-transmission unit allows for long-range operation. (ii) Measurements of intracranial pressure over three days reveal accurate, consistent responses (red) from bioresorbable devices encapsulated with biodegradable polyanhydride, when compared with the data from a commercial sensor (blue). Reproduced with permission from [148]. (D) Synthetic schemes of the thiol-acrylate-based polymer and its chemical modification via oxidation. Selective oxidation in the polymer demonstrates the rigidity contrast. Reproduced with permission from [152]. (E) 3D-multifunctional membranes for the spatiotemporal measurement across the entire epicardial surface. The bottom row shows the ECG sensor, Si strain gauge, microscale inorganic light-emitting diodes, pH sensor, and temperature sensor. Reproduced with permission from [156]. (F) Images of lead zirconate titanate (PZT) mechanical energy harvester co-integrated with a rectifier and rechargeable battery, mounting on the right ventricle of a bovine heart during (Left) expansion and (Right) relaxation. Reprinted with permission from [158]. (For interpretation of the references to color in this figure legend, the reader is referred to the web version of this article.)

electrophysiological signals from the cortical surface and the subgaleal space *in vivo* [137]. Capable of detecting normal physiologic and epileptiform activities from both acute and chronic recordings, the bioresorbable silicon electrodes open up new opportunities such as postoperation monitoring of brain activity, with direct relevance to clinical practice. Wireless monitoring of intracranial pressure and temperature from freely moving animals can also be achieved by the bioresorbable silicon electronic sensors, promising the use of these devices for the treatment of traumatic brain injury (Fig. 5C) [138].

Depending on the architecture and application of different device systems, the materials and methods to fabricate these bio-

integrated devices vary widely. The manufacturing methods of the high-performance inorganic bio-integrated devices can be broadly classified into two types: 1) direct manufacturing on the target substrate, or 2) transferring the fabricated devices from conventional wafer substrate to the target. Because of the temperature requirement of the target substrate (i.e., the glass temperature of the substrate to be higher than the processing temperature), the former is limited by the ranges of processes and substrate materials. Though the latter is versatile, its typical involvement of the photolithographic processes complicates the manufacturing steps. In an attempt to address the challenge, different manufacturing methods are actively being developed for the cost-effective large-scale production of the bio-integrated devices, including blade cutting [139], laser cutting [140], and laser-induced porous graphene [141]. Opportunities also emerge when materials with new functionalities are explored in the manufacturing processes. For instance, the use of a polymer substrate with a programmable rigidity results in the capability to directly manufacture bio-integrated devices [142], eliminating the need for transfer printing while significantly enhancing the effect of strain isolation [143]. The polymer is synthesized via the thiol-acrylate click chemistry, and spatially confined oxidation creates rigid island regions for direct device fabrication (Fig. 5D). When it comes to the manufacturing of bioresorbable electronics, various processing and manufacturing techniques would need to be adapted for the biodegradable materials, as discussed in a recent review article [144].

Stretchable multiplexed devices capable of high-density mapping provide a valuable experimental and clinical tool to identify the onset and monitor the progression of arrhythmia mechanisms [145]. The explanted Langendorff-perfused rabbit hearts integrated with the stretchable device throughout the entire epicardial surface can perform high-density multiparametric physiological mapping and stimulation (Fig. 5E) [146,147]. The representative device includes Au electrodes for electrical sensing and stimulation, Au resistors for temperature sensing and heating, microscale inorganic light-emitting diodes for optical mapping, Si strain gauge for strain measurement, and iridium oxide pads for pH sensing. The high-density array allows the device to probe the local information with a high spatiotemporal resolution on the metabolic, ionic, thermal, excitable, contractile states for cardiac diagnostics and therapy. The energy requirement is not a limiting factor for the use of bio-integrated devices in the experimental study of explanted organs, but it is indeed a concern for electrically implanted devices such as pacemakers and defibrillators. As an alternative to the battery power, piezoelectric energy harvesting and storage that can harvest the energy from the natural processes of the body presents an attractive opportunity [148]. Integrated with rectifiers and microbatteries, the use of lead zirconate titanate could convert the electrical energy from the natural contractile and relaxation motions of the heart, lung, and diaphragm (Fig. 5F), reducing the battery size and eliminating the need to replace them. The energy harvesting units or others based on wireless energy transmission such as ultrasound [149] would be particularly attractive for cardiac pacemakers by eliminating the thrombogenic leads [150].

4.2. Electronic-mechanical assemblies for smart drug delivery

The traditional drug delivery approaches are based on either organic or inorganic materials, including liposomes [151,152], hydrogels [153], dendrimer [154,155], nanoparticles [156], and 2D materials [157]. The drug delivery could be triggered by internal (e.g., pH level [158], temperature [159,160], redox conditions [161], and glucose level [162]) or external (e.g., magnetic field [135,163], light [155,164], strain [165], ultrasound [166], and electric field [167]) signals. The lack of analysis of drug doses and their therapeutic effect calls for the "smart" drug delivery devices (DDD) that could extract long-term pathophysiological conditions from individual patients. Recent efforts include the development of bio-integrated microneedles and conformal transdermal drug delivery systems.

Since the early effort in the late 1990s, a variety of materials and manufacturing methods have been developed to create microneedles [168] that feature painless drug delivery by avoiding the pain receptors at the epidermis, upon the trigger of different stimuli. As one representative example, using near-infrared trigger minimizes the damage to the skin [164]. The closed loop feedback system is highly desirable for drug delivery. In such a system, the real-time physiological condition of patients monitored by the sensor could be used to trigger self-regulated organ- or tissue-specific drug release, enabling precise control of drug dose at the predetermined physiological conditions without the intervention of doctors. The self-regulated delivery of anticoagulant drugs (e.g., heparin) is achieved by integrating thrombin-responsive polymer-drug conjugate into a disposable microneedle array for auto-regulation of blood coagulation (Fig. 6A, i) [169]. Upon thrombin activation, the thrombin-cleavable peptides promptly release heparin from the backbone of hyaluronic acid, and the released heparin is trapped in the polymer matrix without elevated thrombin concentration. Therefore, the microneedle patch will rapidly respond to the increased thrombin level and release the corresponding dose of anticoagulant to inhibit the coagulation activation. The released heparin also inactivates thrombin and suppresses the further release of heparin, preventing bleeding complications or spontaneous hemorrhages from the over-dosage of heparin. A pulsatile release is also observed when the hydrogel is alternatively exposed to solutions with and without heparin (Fig. 6A, ii). By exploring a dual responsive diblock copolymer consisting of poly (ethylene glycol) and polyserine modified with 2-nitroimidazone via a thioether moiety, the microneedle system also demonstrates an insulin delivery loop with enhanced response to the glucose [170]. Capable of responding to both H_2O_2 and hypoxia that are generated from glucose oxidation catalyzed by glucose oxidase (GOx), the insulin-loaded vesicles formed by the diblock copolymer can disassociate and release insulin. Also, the vesicle could eliminate excessive H_2O_2 to minimize the local inflammation and reduce the activity of GOx (Fig. 6B, i). Immersing the insulin-loaded vesicle in the normal and hyperglycemic solutions yields a pulsatile release profile of insulin, showing the sensitivity of the self-regulated insulin delivery system (Fig. 6B, ii).

Besides microneedles, other non-invasive transdermal drug delivery methods also include those based on diffusion [171] with the help of benign chemical enhancers (e.g., urea, fatty acid, and pyrrolidone) or skin irritant organic solutions such as dimethyl sulfoxide (DMSO), dimethylformamide (DMF), and oxazolidinone [172]. Because effective diffusion of drugs through the epidermal barrier into the blood circulation system is limited by their molecular weight and partition coefficient [173], various chemical (e.g., the use of emulsion-based carriers [174] and nano-carriers [175]) and physical (e.g., electrical [176], thermal [177], and ultrasound [178]) methods have been explored to facilitate the transport through the epidermis. Based on iontophoresis [179], a patch-like drug delivery system can drive the charged drug molecules to penetrate through the skin with enhanced penetration depth (over the one based on thermal diffusion), because of the repulsion force between them and the electrode (Fig. 6C) [180]. By employing the high surface-to-volume ratio mesoporous silica nanoparticles (MSN) as the drug delivery vehicle, a high drug loading is achieved. It should be noted, however, that the molecular weight and transport efficiency are still limited in many transdermal drug delivery

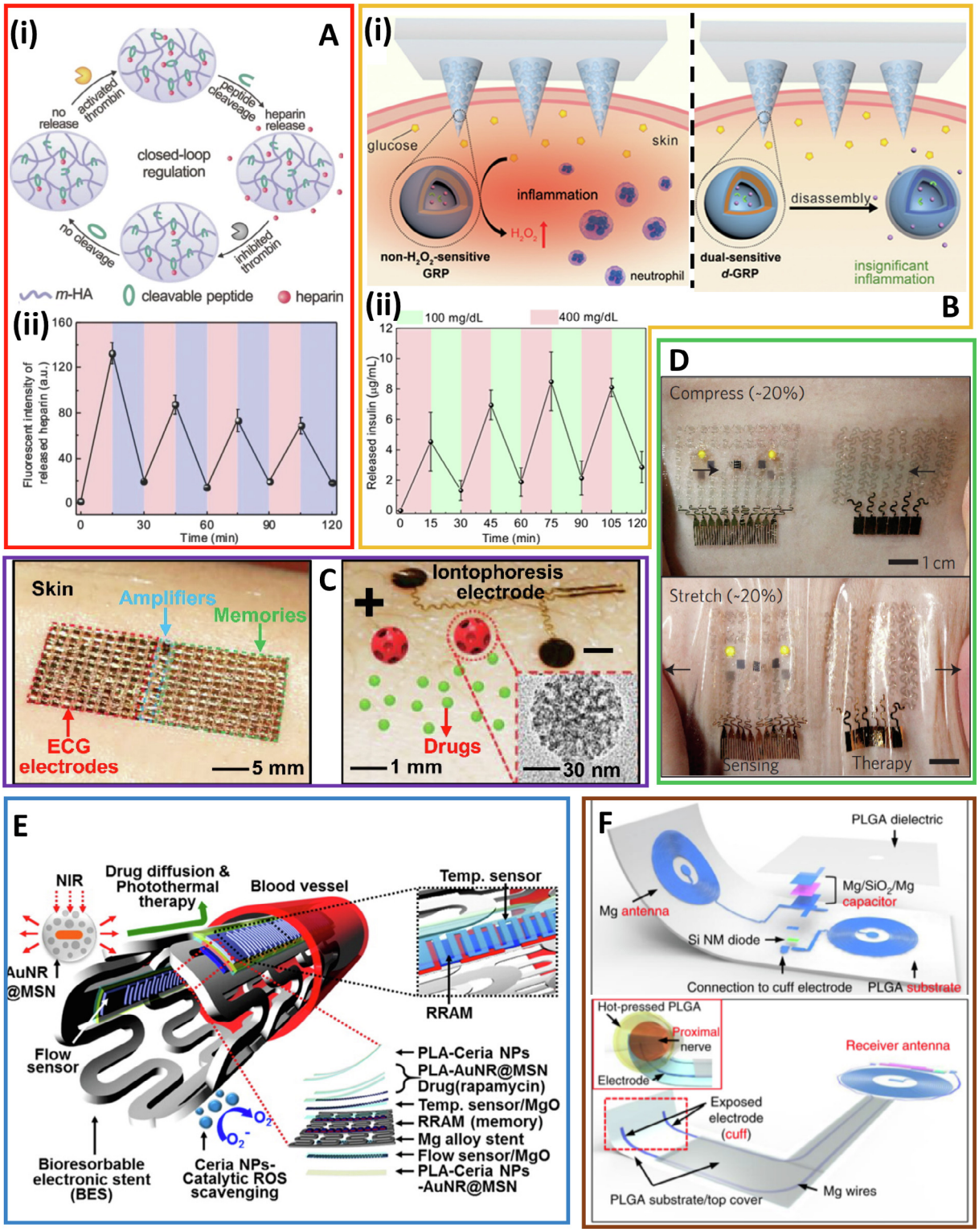

Fig. 6. (A) Closed-loop regulation of (i) the heparin delivery system that is based on thrombin-responsive heparin-conjugated hyaluronic acid (TR-HAHP) and (ii) the heparin release profile from the TR-HAHP. Reprinted with permission from [184]. (B) (i) Schematic illustration of the drug release process of non-H_2O_2-sensitive glucose responsive polymersome-based (GRP) vesicles and the dual responsive glucose responsive polymersome-based vesicles (d-GRP). The dual sensing mechanism of the d-GRP effectively reduces the local inflammation. (ii) A pulsatile insulin release profile is obtained from the d-GRP samples. Reprinted with permission from [185]. (C) ECG electrodes, amplifiers, and memories mounted on the skin for ECG measurement and transdermal drug delivery. Drug diffusion length is significantly improved by the use of iontophoresis. Reprinted with permission from [196]. (D) Optical images of the diabetes patch laminated on the human skin under mechanical deformations. Reprinted with permission from [198]. (E) Schematic illustration of the bioresorbable electronic stent (BES) with its top view and the layer information. The BES includes bioresorbable temperature/flow sensors, memory modules, and bioresorbable/bioinert therapeutic nanoparticles. The therapeutic functions are either passive (ROS scavenging) or actively actuated (hyperthermia-based drug release) by a near-infrared (NIR) laser exposure. Reprinted with permission from [199]. (F) Schematic illustration of a bioresorbable, wireless electrical stimulator as an electronic neuroregenerative medical device. The electronic component is a wireless receiver acting as a radio frequency power harvester, built with an Mg inductor, a Si NM radio frequency diode, an Mg/SiO2/Mg capacitor, and a PLGA substrate interconnected with Mg deposited by sputtering (top). Folding the constructed system in half yields a compact device with a double-coil inductor. The bottom presents the electrode and cuff interface for nerve stimulation, consisting of metal electrodes embedded in a PLGA substrate with a PLGA encapsulation layer. Rolling the end of the system into a cylinder creates a cuff with exposed electrodes at the ends as an interface to the nerve. Reprinted with permission from [124].

systems and that certain high molecular weight drugs (e.g., insulin) still require the use of microneedles. Sensing and actuation components also need to be integrated into a closed loop feedback system to provide a self-regulated system for precise control of drug delivery. Based on the real-time correction of the measured blood glucose level (against pH, temperature, and humidity values), a closed loop feedback system is designed to deliver metformin [181,182]. Metformin-loaded phase change nanoparticles are embedded in hyaluronic acid hydrogels microneedles, which are further encapsulated with phase change materials. Actuating the microneedles with an integrated heater induces the drug release. Due to the high electron mobility, flexibility, and optical transparency, graphene doped with gold has been exploited in fabricating electrochemical sensors for the detection of pH, humidity, and glucose levels. Coupling the sensing module with a therapy platform yields a wearable diabetes patch that can have conformal contact with human skins even with mechanical deformation (Fig. 6D).

Specific applications may also require the biodegradable systems for drug delivery. A recent study demonstrates a bioresorbable electronic stent that integrates the drug delivery system and various sensing components (Fig. 6E) [183]. The perfusion by percutaneous coronary interventions (PEI) generates reactive oxygen species (ROS). Exploring the ceria nanoparticles (ceria NPs) to scavenge ROS reduces the inflammation and the risk to cause instent thrombosis. The drug loaded in the gold nanorod core/mesoporous silica nanoparticle shell (AuNR@MSN) can be activated by the external optical stimulus to trigger local release. The potential use of bioresorbable electronic implants in the endovascular system is demonstrated through the *ex vivo* and *in vivo* animal experiments. Specific sensors can also be explored as actuators for nonpharmacological therapy. For instance, a temperature resistor can serve as a heater for thermal treatment when power is supplied [113]. The mode of therapy also goes beyond thermal to electrical stimulation. Programmed electrical stimulation represents an effective means for the management of critical nerve injuries. The neuroregenerative bioelectronics interventions (i.e., nerve stimulation) are applied by connecting a radio frequency power harvester to an electrode and cuff interface (Fig. 6F) [184]. In addition to the enhanced neuroregeneration and functional recovery of injured nervous tissue in rodent models, these bioelectronic devices could have broad applicability to various tissues and organs in the clinical practice.

4.3. Biocompatibility and foreign body response

As the mechanism of biocompatibility and relevant approaches have been thoroughly reviewed [185–187], we will only provide a brief overview of the highlights in the following discussion. In the application of *in vitro* cell culture and drug screening, inappropriate selection of materials used in the electronic-mechanical assemblies may cause cells apoptosis, trigger cells signaling pathway, and induce cascades. Thus, biocompatible material coatings have been commonly used to address the challenge. This general approach has also been applied to the application of epidermal electronics in the bio-integrated devices. By exploring biocompatible substrate and encapsulation for the epidermal electronics to interface with the skin, allergies could be avoided. In direct contrast to the examples above, the biocompatibility coupled with foreign body response becomes particularly challenging when it comes to the implantable devices. It is worth noting that the foreign body response to one specific material may widely vary from one site to another. The site-dependent foreign body response indicates that biocompatibility is not solely dependent on the property of materials itself. Therefore, there is no silver bullet in the design of biocompatible materials that could address all of the biomedical applications. In addition to biocompatible material coatings, other approaches to overcome the host response have also been reviewed [188], such as steroidal and nonsteroidal anti-inflammatory drugs, or angiogenic drugs. The former inhibits the formation and secretion of inflammatory mediators to suppress the immune response, but long-term systemic use of these drugs results in unwanted side effects. The latter promotes angiogenesis to improve analyte transport, which also helps heal the trauma caused during implantation. In this regard, biocompatibility has been perceived to be the ability of a device to perform with an appropriate host response in a specific situation [187]. The evoked host-response include protein adsorption, platelet adhesion, cytotoxic effects, clotting cascade, antibody production, and tissue-specific cell responses [187].

The challenge of foreign body response comes from the fact that the complicated interaction between various materials (e.g., metals, alloys, polymers, and ceramics) and the biological system depends on various properties of the material, including the composition, structure, surface chemistry, surface topography, surface energy, porosity, or degradation profile for the degradable material. The evoked foreign body response can in return alter the properties of the material [187]. Due to the complexity of the foreign body response, the biocompatibility of the electronic-mechanical assemblies can hardly be determined with an *in vitro* test. The most reliable method to examine the biocompatibility lies in the clinical trials. However, clinical trials are not practical for every single study. To help ease the situation, the selection of the materials used in the electronic-mechanical assemblies could start to reference those in the existing implantable devices summarized in several review articles [189–193]. The representative examples include the use of alumina in joint replacement, calcium phosphate in bone substitutes, polyurethane in catheters, and silicone rubber in soft tissue augmentation. Under regulatory guidelines (FDA ISO 10993 [194]), a list of materials that include silicon, polysilicon, SiO_2, Si_3N_4, and SiC has been tested and reported to have minimum biocompatibility issues [195]. Also, microfabricated implantable devices have also commonly explored other biocompatible materials, including cobalt-chromium, titanium, platinum, nitinol, parylene C, polymethylmethacrylate (PMMA), and polyimide [196]. In the application of transient electronics, biocompatibility and bioresorption have been demonstrated in both *in vitro* and *in vivo* investigations of various inorganic materials, including Si nanomembranes [197,198], Mg/MgO on silk [197], W [198], Fe [199], poly-Si/a-Si/SiGe/Ge [124], and silicate spin-on-glass [200]. Interests also arise in biodegradable materials with natural origin such as silk [130], gelatin [131], shellac [201], pullulan [202], and egg albumen [203]. Though foreign body response is complicated, an in-depth understanding of how the immune system interacts with the electronic-mechanical assemblies [204] may provide critical insights to the biocompatibility and function of the assemblies.

5. Conclusion and outlook

In this short review, we first provide an overview of the recent progress on the integration of cells and tissues with both electronic and mechanical assemblies. The cells and organoids are integrated with various sensing modules in microfluidics, providing a unique platform for disease modeling and drug development. However, the cells and organoids explored in most of the studies are limited in size due to the lack of 3D structures and vascular networks. In an attempt to address this challenge, bioprinting has been utilized to build 3D tissue constructs with vascular networks, which would be essential to realizing large-size, functional 3D tissues and organs. As an alternative, the mechanically guided assembly has also been exploited as tissue scaffolds. As this approach uses the advanced

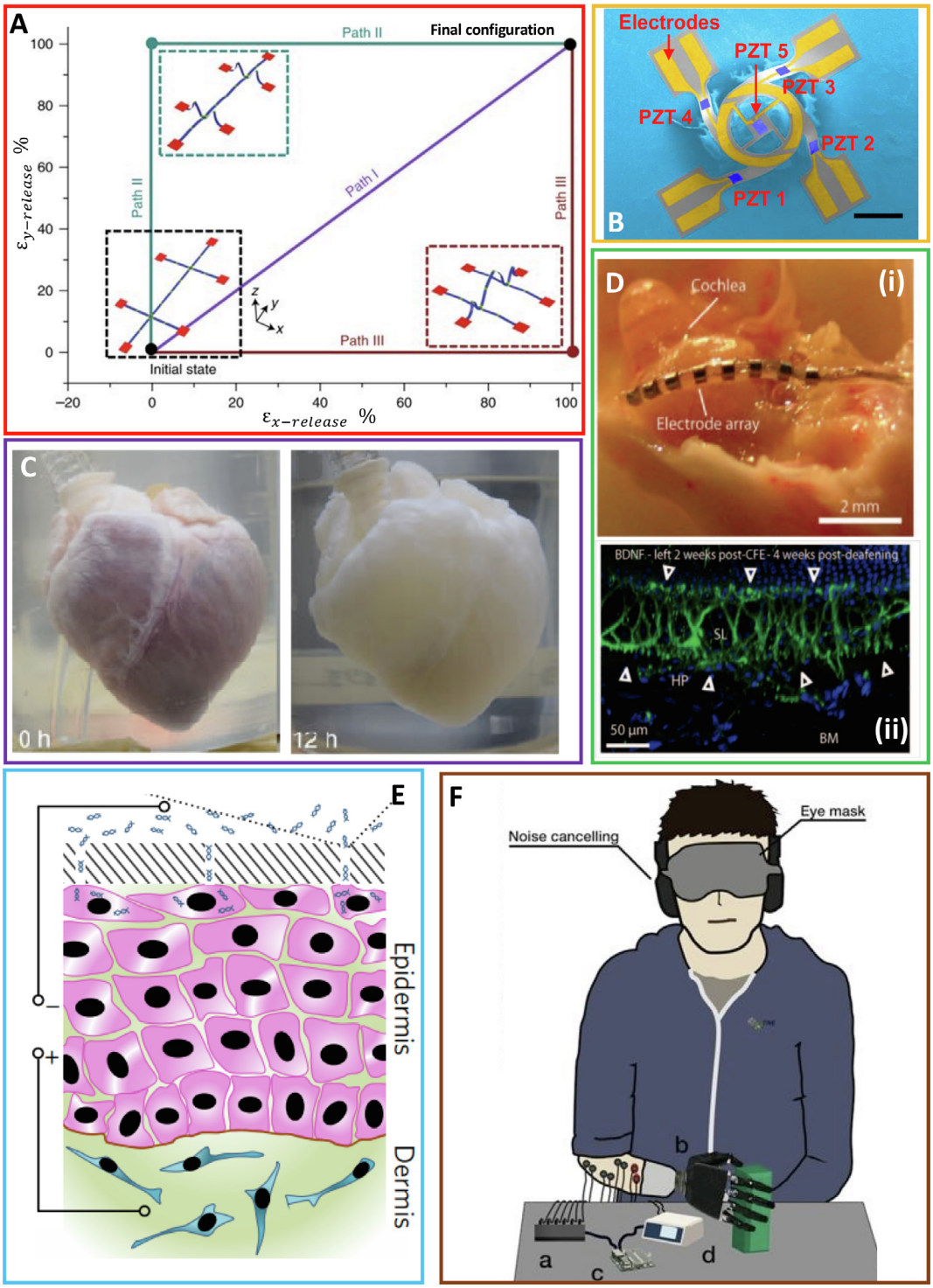

Fig. 7. (A) Morphable 3D structures with different stable states by following different sequential release paths. Reproduced with permission [203]. (B) SEM image of the representative 3D structure consisting of five independently addressable PZT microactuators. Reproduced with permission [206]. (C) Porcine heart before and after decellularization. Reproduced with permission [212]. (D) (i) 8-node cochlear electrodes placed on the cochlea of guinea pig. (ii) Fluorescent image of peripheral spiral ganglion neurites 4 weeks after close field electroporation. Reproduced with permission from [216]. (E) Schematic of the tissue nano-transfection process on skins through electroporation. Reproduced with permission from [220]. (F) Schematic overview of the experimental setup for bidirectional hand prosthesis. (a, b, c, and d represent data acquisition system, robotic hand, an embedded computer, and stimulator, respectively). Reproduced with permission from [227].

materials, the sensors and actuators can be readily integrated to serve as an electronic-mechanical assembly.

Though great strides have been made, there still exist opportunities for the use of mechanically guided assembly and 3D/4D bioprinting. One example in the former is that the assembled 3D structures are usually in the first-order buckling modes with the lowest strain energy. As for the designs with sufficiently close first- and second-order modes, incorporating a patterned film with well-defined residual stresses at strategic locations in the 2D precursor enables the system to select high-order buckling modes or

to enhance the yield of the lowest order mode [205]. As a way to bypass the need for the pre-stretched platform, a tensile buckling strategy can create additional classes of 3D geometries and a strain sensor with visible readout from LEDs is demonstrated to detect large strain range through an array of mechanically triggered electrical switches [206]. Applying the class of 3D structures in the form of vibratory platforms also extends their application toward resonators with tunable resonant frequency and potentially as energy harvesters as well [207]. Similar to the concept of 4D printing but without the use of stimuli-responsive materials, the 3D structures can morph into two or multiple distinct stable shapes through different loading paths (e.g., simultaneous vs. sequential release) (Fig. 7A). The design strategies have been demonstrated in a 3D radiofrequency switch and a concealable electromagnetic device [208].

Additional opportunities exist when the mechanically assembled 3D structures are integrated with other advanced functional materials and devices. Other routes to assemble advanced functional materials into 3D structures across a range of length scales can be found in a recent review article [16]. Integrating two-dimensional semiconductor/semi-metal materials (e.g., graphene and MoS_2) on the mechanically assembled three-dimensional systems allows photodetection and light imaging that can measure the direction, intensity, and angular divergence properties of the incident light [209]. It is also possible to directly embed high-performance electronic devices such as those based on silicon nanomembranes (Si NMs) released from commercial wafer sources into the resulting 3D structures [210]. The demonstrated examples include n-channel Si NM MOSFETs (nMOS), Si NM diodes, and p-channel silicon MOSFETs (pMOS) on interconnected bridges, coils, and extended chiral structures. When incorporating multiple, individually addressable piezoelectric thin film actuators, active vibratory excitations with precise control can provide 3D mesostructures a unique capability toward biosensing and mechanobiology among many others [211]. Strategic designs of the 3D structures can yield two quantitatively different and well-separated resonant modes corresponding to the twisting motion and the piston-type vibration, respectively. With decoupled sensitivities to viscosity and density in these two modes, the 3D structures can simultaneously extract the viscosity and density of various liquids including biological, complex, and time-variant fluids with high precision (Fig. 7B). Due to the deformability of the 3D structures and their compliant supports, the conformal bonding of these 3D structures onto the medical devices (e.g., cardiovascular stents, flexible catheters, and balloon catheters) demonstrates their potential use as integrated sensors. Certain electronic-mechanical assemblies integrated on the biological system at a given length scale could also be explored for the application at a different length scale. For instance, the use of mechanically assembled 3D structures also goes beyond the mechanical assemblies for tissue culture to the stretchable interconnection in constructing bio-integrated electronics for interfacing with the living individual. In comparison to a planar 2D serpentine, the 3D coils from the mechanical guided assembly have a nearly decoupled deformation from the elastomeric substrate to yield significantly improved stretchability, enabling their use as interconnect network to connect chip-scale components for bio-integrated electronics when combined with a two-stage encapsulation strategy [212].

Though powerful in disease modeling and drug screening, the organoids are still different from their corresponding organs. Capable of providing vascular networks, the bioprinting represents a versatile tool for organ regeneration [73,213], or even to construct functional organs. But it should be noted that there are few demonstrations on the integration of bioprinted tissues and models with sensors and actuators for simultaneous monitoring and functional stimulation. Though this integration is still at its infancy, the potential opportunities would undoubtedly open up wide-ranging applications far beyond the current disease modeling with organoids. As an alternative approach to the 3D/4D bioprinting, decellularization and recellularization have been explored to construct biomimetic human whole organs, including kidney [214], liver [128], lung [215], and heart [216]. With efficient cell removal and ECM retention, the decellularized ECM scaffold is employed for seeding human cells to reconstruct the whole human organ [217] (Fig. 7C). The demonstrated seeding human cells include fatal/adult cells, embryonic stem cells, mesenchymal stem cells, and induced pluripotent stem cells. As in the cell culture, culturing of the seeded cells requires various proper cues, suggesting the need for the sensing modules in the recellularization process. Though a bioreactor for the whole-heart cultivation is constructed to monitor multiple parameters (e.g., temperature, pH level, and dissolved oxygen concentration [218]), the system still cannot probe the local information. Moreover, a mechanical stimulus to facilitate the maturation process of the seeded heart is provided by inserting and periodically varying the inner pressure of a balloon, which could be simplified when integrated actuators are in place.

The bio-integrated electronics have shown great potential in implantable devices even beyond those covered in the current discussion. Capable of transducing the frequency components of sound and stimulating the spiral ganglion neurons with current pulses in real-time, cochlear implants have been approved for adults with a severe hearing loss by the FDA over decades [219]. Among the widely acknowledged challenges [220], attention has been given to the neuron-electrode interface for improving the performance of cochlear implants. As an effective method for gene delivery, the electroporation with cochlear electrodes is exploited to drive the expression of brain-derived neurotrophic factors for better regeneration of spiral ganglion neurons [221]. Upon implantation of the eight-node cochlear electrodes into the exposed scala tympani of a guinea pig through the round window followed by close field electroporation, gene therapy induces regeneration of peripheral spiral ganglion neurites bordering the spiral limbus within the scala media, in direct contrast to the control group (Fig. 7D). Introducing gene materials (e.g., DNAs and RNAs) into cells is also of critical importance for gene editing, cell reprogramming, and immunotherapy [222–224]. It has been a challenge to precisely manipulate the delivery pathway over the cell membrane for the engineered cargos (e.g., reprogramming factors or CRISPR-Cas9) that are typically associated with large molecular weights (>6 kbps) [225]. Relying on the electroporation through nanochannels, the device in direct contact with the skin of mouse 'electrophoretically' drives reprogramming factors with large-molecular-weight into epidermal cells for *in vivo* cell reprogramming (Fig. 7E) [226]. Reprogramming skin cells into induced endothelial cells rapidly forms blood vessel networks to restore tissue and limb perfusion in two murine models of injury-induced ischemia.

The application of bio-integrated devices also goes beyond healthcare to human-machine interfaces. The measured data obtained from wide-ranging areas of the body with the bio-integrated devices can be used for advanced forms of human-machine interface and control. Signals of surface electromyograms measured from four different bimanual gestures on the forearms are classified into distinct commands to operate the quadrotor remotely [227]. Non-invasive recording of electroencephalograms also expands the opportunity from diagnosis of neurological disorders to brain-computer interfaces. The bio-integrated devices can avoid the irritation and irreversible degradation at the skin interface, thereby enabling the high-fidelity and long-term capture of electroencephalograms. The proof-of-concept brain-computer interface based on a steady-state visually evoked potential demonstrates its utility in a text speller [228]. As a related example, smart

prostheses represent another opportunity for the integration of living individuals with electronic-mechanical assemblies. Successfully commercialized, hand prostheses can collect superficial electromyogram from the upper limb with electrodes and then transduce the signal to drive the motion of the hands for performing daily tasks. Due to the lack of sensory module needed in a feedback loop, their function is limited to actuation. One solution is to integrate electrodes into the residual limb to stimulate the nerves [229]. Attempts on non-invasive somatotopic sensitive hand prostheses also include the use of mechanical [230], electrical [231], and auditory [232] feedback modalities. For instance, the transcutaneous electrical stimulation is shown to elicit successful sensing of object position in the hands of amputees, which is then used to adjust the force exerted by prosthetic hand through the sensory feedback (Fig. 7F). The smart prostheses with a closed loop feedback control would expand the application opportunities for the human-machine interface. It would also be of great interest to monitor the residual limb health in persons who wear prostheses. Integrating the sensing modules with skin-like properties would advance the person-centered prosthetic care.

Although the recent advances in the bio-integrated devices centered in research laboratories, there is a growing interest at companies to commercialize the technology in clinics and consumer products. To assess real-world health outcomes, the Kintinuum™ system developed by MC10® (Lexington, MA, USA) could quantify treatment efficacy through a combination of patient-reported subjective data and objective data collected from wearable sensors that conform to the human body for maximum patient conform. Naturally conforms to the contours of the human body, the BioStampRC® system reduces observation error for improved data capture, while allowing study subjects to move comfortably through regular activities in clinical or remote settings. As a successor, BioStamp nPoint® is an FDA 510(k) cleared medical device designed to collect clinical metrics including vital signs, activity and posture classification, sleep metrics, and many others. The NeuroLux Optogenetics System developed by NeuroLux® (Evanston, IL, USA) provides the researcher and relevant communities with the lightweight, ultra-miniaturized, battery-free brain implantable device and spinal device to investigate neuroscience. Several other start-up companies have recently started to commercialize the bio-integrated and implantable devices, such as Wearifi® (Champaign, IL, USA) to develop the wearable wireless devices by leveraging the near-field communication technology and Transient Electronics Inc.® (Brookline, MA, USA) to produce an implantable transient electronic nerve stimulation device. Also, advanced manufacturing approaches in fabricating the bio-integrated and implantable devices create pathways to commercialization with time scale much shorter than those microfabricated devices derived from the academic research. The commercialization time scale is also largely dependent on the testing of biocompatibility regulated by the Food and Drug Administration (FDA) guidelines [194]. As the fabrication process needs to be completed before the examination, the fabrication method should also be biocompatible. As one representative example, the high level of manufacturing residues could cause adverse effects, which results in the FDA to recall hip prosthesis produced by Zimmer® (Warsaw, IN, USA) in 2015. Nevertheless, the broad range of interesting scientific topics combined with the translational impact and industrial relevance motivates expanded efforts in the burgeoning field of integration of biological systems with electronic-mechanical assemblies.

Acknowledgments

The authors would like to thank the start-up fund at The Pennsylvania State University, the Doctoral New Investigator grant from the American Chemical Society Petroleum Research Fund, NIH Director's New Innovator Award 1DP2EB020549-01, and NSF MME program grant # 1642186 for financial support.

References

[1] J.L. Ruan, N.L. Tulloch, M. Saiget, S.L. Paige, M.V. Razumova, M. Regnier, K.C. Tung, G. Keller, L. Pabon, H. Reinecke, Mechanical stress promotes maturation of human myocardium from pluripotent stem cell-derived progenitors, Stem Cells 33 (7) (2015) 2148–2157.
[2] M.P. Willand, M.-A. Nguyen, G.H. Borschel, T. Gordon, Electrical stimulation to promote peripheral nerve regeneration, Neurorehabil. Neural Repair 30 (5) (2016) 490–496.
[3] H. Lin, Y. Tang, T.P. Lozito, N. Oyster, R.B. Kang, M.R. Fritch, B. Wang, R.S. Tuan, Projection stereolithographic fabrication of BMP-2 gene-activated matrix for bone tissue engineering, Sci. Rep. 7 (1) (2017) 11327.
[4] R. Trombetta, J.A. Inzana, E.M. Schwarz, S.L. Kates, H.A. Awad, 3D printing of calcium phosphate ceramics for bone tissue engineering and drug delivery, Ann. Biomed. Eng. 45 (1) (2017) 23–44.
[5] G. Gaal, M. Mendes, T.P. de Almeida, M.H. Piazzetta, Â.L. Gobbi, A. Riul Jr, V. Rodrigues, Simplified fabrication of integrated microfluidic devices using fused deposition modeling 3D printing, Sens. Actuat. B Chem. 242 (2017) 35–40.
[6] S.L. Sing, W.Y. Yeong, F.E. Wiria, B.Y. Tay, Z. Zhao, L. Zhao, Z. Tian, S. Yang, Direct selective laser sintering and melting of ceramics: a review, Rapid Prototyping J. 23 (3) (2017) 611–623.
[7] S.C. Cox, J.A. Thornby, G.J. Gibbons, M.A. Williams, K.K. Mallick, 3D printing of porous hydroxyapatite scaffolds intended for use in bone tissue engineering applications, Mater. Sci. Eng. C 47 (2015) 237–247.
[8] H.H. Malik, A.R. Darwood, S. Shaunak, P. Kulatilake, A. Abdulrahman, O. Mulki, A. Baskaradas, Three-dimensional printing in surgery: a review of current surgical applications, J. Surg. Res. 199 (2) (2015) 512–522.
[9] S.J. Trenfield, A. Awad, A. Goyanes, S. Gaisford, A.W. Basit, 3D printing pharmaceuticals: drug development to frontline care, Trends Pharmacol. Sci. (2018).
[10] C.B. Highley, C.B. Rodell, J.A. Burdick, Direct 3D printing of shear-thinning hydrogels into self-healing hydrogels, Adv. Mater. 27 (34) (2015) 5075–5079.
[11] H. Cui, R. Hensleigh, D. Yao, D. Maurya, P. Kumar, M.G. Kang, S. Priya, X. Zheng, Three-dimensional printing of piezoelectric materials with designed anisotropy and directional response, Nat. Mater. (2019).
[12] Z. Yan, M. Han, Y. Shi, A. Badea, Y. Yang, A. Kulkarni, E. Hanson, M.E. Kandel, X. Wen, F. Zhang, Three-dimensional mesostructures as high-temperature growth templates, electronic cellular scaffolds, and self-propelled microrobots, Proc. Natl. Acad. Sci. U.S.A. 114 (45) (2017) E9455–E9464.
[13] Q. Zhang, F. Zhang, S.P. Medarametla, H. Li, C. Zhou, D.J.S. Lin, 3D printing of graphene aerogels, Small 12 (13) (2016) 1702–1708.
[14] S. Xu, Z. Yan, K.I. Jang, W. Huang, H.R. Fu, J. Kim, Z. Wei, M. Flavin, J. McCracken, R. Wang, A. Badea, Y. Liu, D.Q. Xiao, G.Y. Zhou, J. Lee, H.U. Chung, H.Y. Cheng, W. Ren, A. Banks, X.L. Li, U. Paik, R.G. Nuzzo, Y.G. Huang, Y.H. Zhang, J.A. Rogers, Assembly of micro/nanomaterials into complex, three-dimensional architectures by compressive buckling, Science 347 (6218) (2015) 154–159.
[15] Z. Yan, M. Han, Y. Yang, K. Nan, H. Luan, Y. Luo, Y. Zhang, Y. Huang, J.A. Rogers, Deterministic assembly of 3D mesostructures in advanced materials via compressive buckling: A short review of recent progress, Extreme Mech. Lett. 11 (2017) 96–104.
[16] X. Ning, X. Wang, Y. Zhang, X. Yu, D. Choi, N. Zheng, D.S. Kim, Y. Huang, Y. Zhang, J.A. Rogers, Assembly of advanced materials into 3D functional structures by methods inspired by origami and kirigami: a review, advanced materials, Interfaces (2018) 1800284.
[17] Y. Zhang, F. Zhang, Z. Yan, Q. Ma, X. Li, Y. Huang, J.A. Rogers, Printing, folding and assembly methods for forming 3D mesostructures in advanced materials, Nat. Rev. Mater. 2 (4) (2017) 17019.
[18] R.G. Harrison, The outgrowth of the nerve fiber as a mode of protoplasmic movement, J. Exp. Zool. 9 (4) (1910) 787–846.
[19] S.N. Bhatia, D.E. Ingber, Microfluidic organs-on-chips, Nat. Biotechnol. 32 (8) (2014) 760.
[20] M. Mehling, S. Tay, Microfluidic cell culture, Curr. Opin. Biotechnol. 25 (2014) 95–102.
[21] A. Cipitria, M. Salmeron-Sanchez, Mechanotransduction and growth factor signalling to engineer cellular microenvironments, Adv. Healthcare Mater. 6 (15) (2017).
[22] B.D. Riehl, J.-H. Park, I.K. Kwon, J.Y. Lim, Mechanical stretching for tissue engineering: two-dimensional and three-dimensional constructs, Tissue Eng. Part B Rev. 18 (4) (2012) 288–300.
[23] Q. Wei, C. Huang, Y. Zhang, T. Zhao, P. Zhao, P. Butler, S. Zhang, Mechanotargeting: mechanics-dependent cellular uptake of nanoparticles, Adv. Mater. 1707464 (2018).
[24] R. Balint, N.J. Cassidy, S.H. Cartmell, Electrical stimulation: a novel tool for tissue engineering, Tissue Eng. Part B 19 (1) (2013) 48–57.
[25] W. Zhang, Y.S. Zhang, S.M. Bakht, J. Aleman, S.R. Shin, K. Yue, M. Sica, J. Ribas, M. Duchamp, J. Ju, Elastomeric free-form blood vessels for interconnecting organs on chip systems, Lab on A Chip 16 (9) (2016) 1579–1586.
[26] H. Liu, L.A. MacQueen, J.F. Usprech, H. Maleki, K.L. Sider, M.G. Doyle, Y. Sun, C. A. Simmons, Microdevice arrays with strain sensors for 3D mechanical

stimulation and monitoring of engineered tissues, Biomaterials 172 (2018) 30–40.
[27] Z. Wang, L. Tan, X. Pan, G. Liu, Y. He, W. Jin, M. Li, Y. Hu, H. Gu, Self-powered viscosity and pressure sensing in microfluidic systems based on the piezoelectric energy harvesting of flowing droplets, ACS Appl. Mater. Interfaces 9 (34) (2017) 28586–28595.
[28] Y. Chen, H.N. Chan, S.A. Michael, Y. Shen, Y. Chen, Q. Tian, L. Huang, H. Wu, A microfluidic circulatory system integrated with capillary-assisted pressure sensors, Lab on A Chip 17 (4) (2017) 653–662.
[29] Y. Xu, X. Xie, Y. Duan, L. Wang, Z. Cheng, J. Cheng, A review of impedance measurements of whole cells, Biosensors and Bioelectronics 77 (2016) 824–836.
[30] A. Uysal, S. Azak, M.C. Colak, O. Burma, I.M. Ozguler, B. Ustundag, M.K. Bayar, Perioperative high-dose amiodarone elevates nitric oxide levels in patients undergoing coronary artery bypass surgery, Biomed. Res. 24 (4) (2013) 486–492.
[31] P.M. Misun, J. Rothe, Y.R. Schmid, A. Hierlemann, O. Frey, Multi-analyte biosensor interface for real-time monitoring of 3D microtissue spheroids in hanging-drop networks, Microsyst. Nanoeng. 2 (2016) 16022.
[32] D. Bavli, S. Prill, E. Ezra, G. Levy, M. Cohen, M. Vinken, J. Vanfleteren, M. Jaeger, Y. Nahmias, Real-time monitoring of metabolic function in liver-on-chip microdevices tracks the dynamics of mitochondrial dysfunction, Proc. Natl. Acad. Sci. U.S.A. 113 (16) (2016) E2231–E2240.
[33] J.R. McKenzie, A.C. Cognata, A.N. Davis, J.P. Wikswo, D.E. Cliffel, Real-time monitoring of cellular bioenergetics with a multianalyte screen-printed electrode, Anal. Chem. 87 (15) (2015) 7857–7864.
[34] I. Taurino, S. Massa, G. Sanzó, J. Aleman, B. Flavia, S.R. Shin, Y.S. Zhang, M.R. Dokmeci, G. De Micheli, S. Carrara, Platinum nanopetal-based potassium sensors for acute cell death monitoring, RSC Adv. 6 (46) (2016) 40517–40526.
[35] Y. Kato, S. Ozawa, C. Miyamoto, Y. Maehata, A. Suzuki, T. Maeda, Y. Baba, Acidic extracellular microenvironment and cancer, Cancer Cell Int. 13 (1) (2013) 89.
[36] S. Lahiri, Historical perspectives of cellular oxygen sensing and responses to hypoxia, J. Appl. Physiol. 88 (4) (2000) 1467–1473.
[37] S.A. Mousavi Shaegh, F. De Ferrari, Y.S. Zhang, M. Nabavinia, N. Binth Mohammad, J. Ryan, A. Pourmand, E. Laukaitis, R. Banan Sadeghian, A. Nadhman, A microfluidic optical platform for real-time monitoring of pH and oxygen in microfluidic bioreactors and organ-on-chip devices, Biomicrofluidics 10 (4) (2016) 044111.
[38] Y.S. Zhang, J. Aleman, S.R. Shin, T. Kilic, D. Kim, S.A.M. Shaegh, S. Massa, R. Riahi, S. Chae, N. Hu, Multisensor-integrated organs-on-chips platform for automated and continual in situ monitoring of organoid behaviors, Proc. Natl. Acad. Sci. U.S.A. (2017) 201612906.
[39] G.A. Giridharan, M.-D. Nguyen, R. Estrada, V. Parichehreh, T. Hamid, M.A. Ismahil, S.D. Prabhu, P. Sethu, Microfluidic cardiac cell culture model (μCCCM), Anal. Chem. 82 (18) (2010) 7581–7587.
[40] R.C. Nordberg, J. Zhang, E.H. Griffith, M.W. Frank, B. Starly, E.G. Loboa, Electrical cell-substrate impedance spectroscopy can monitor age-grouped human adipose stem cell variability during osteogenic differentiation, Stem Cells Transl. Med. 6 (2) (2017) 502–511.
[41] T.A. Nguyen, T.-I. Yin, D. Reyes, G.A. Urban, Microfluidic chip with integrated electrical cell-impedance sensing for monitoring single cancer cell migration in three-dimensional matrixes, Anal. Chem. 85 (22) (2013) 11068–11076.
[42] R. Szulcek, H.J. Bogaard, G.P. van Nieuw Amerongen, Electric cell-substrate impedance sensing for the quantification of endothelial proliferation, barrier function, and motility, J. Visual. Exp. JoVE 85 (2014).
[43] D. Seidel, J. Obendorf, B. Englich, H.-G. Jahnke, V. Semkova, S. Haupt, M. Girard, M. Peschanski, O. Brüstle, A.A. Robitzki, Impedimetric real-time monitoring of neural pluripotent stem cell differentiation process on microelectrode arrays, Biosens. Bioelectron. 86 (2016) 277–286.
[44] T.B. Kornberg, S. Roy, Communicating by touch–neurons are not alone, Trends Cell Biol. 24 (6) (2014) 370–376.
[45] K. Chawla, S.C. Bürgel, G.W. Schmidt, H.-M. Kaltenbach, F. Rudolf, O. Frey, A. Hierlemann, Integrating impedance-based growth-rate monitoring into a microfluidic cell culture platform for live-cell microscopy, Microsyst. Nanoeng. 4 (1) (2018) 8.
[46] B.M. Maoz, A. Herland, O.Y. Henry, W.D. Leineweber, M. Yadid, J. Doyle, R. Mannix, V.J. Kujala, E.A. FitzGerald, K.K. Parker, Organs-on-chips with combined multi-electrode array and transepithelial electrical resistance measurement capabilities, Lab on A Chip 17 (13) (2017) 2294–2302.
[47] T. Sato, H. Clevers, Growing self-organizing mini-guts from a single intestinal stem cell: mechanism and applications, Science 340 (6137) (2013) 1190–1194.
[48] M.A. Lancaster, M. Renner, C.-A. Martin, D. Wenzel, L.S. Bicknell, M.E. Hurles, T. Homfray, J.M. Penninger, A.P. Jackson, J.A. Knoblich, Cerebral organoids model human brain development and microcephaly, Nature 501 (7467) (2013) 373.
[49] N. Khalid, I. Kobayashi, M. Nakajima, Recent lab-on-chip developments for novel drug discovery, Wiley Interdiscipl. Rev. Syst. Biol. Med. 9 (4) (2017) e1381.
[50] P.S. Dittrich, A. Manz, Lab-on-a-chip: microfluidics in drug discovery, Nat. Rev. Drug Discovery 5 (3) (2006) 210.
[51] J. Ahn, J. Ko, S. Lee, J. Yu, Y. Kim, N.L. Jeon, Microfluidics in nanoparticle drug delivery; from synthesis to pre-clinical screening, Adv. Drug Deliv. Rev. (2018).
[52] M.L. McCain, S.P. Sheehy, A. Grosberg, J.A. Goss, K.K. Parker, Recapitulating maladaptive, multiscale remodeling of failing myocardium on a chip, Proc. Natl. Acad. Sci. U.S.A. 110 (24) (2013) 9770–9775.
[53] D. Huh, D.C. Leslie, B.D. Matthews, J.P. Fraser, S. Jurek, G.A. Hamilton, K.S. Thorneloe, M.A. McAlexander, D.E. Ingber, A human disease model of drug toxicity–induced pulmonary edema in a lung-on-a-chip microdevice, Sci. Transl. Med. 4 (159) (2012) 159ra147.
[54] B. Deleglise, S. Magnifico, E. Duplus, P. Vaur, V. Soubeyre, M. Belle, M. Vignes, J.-L. Viovy, E. Jacotot, J.-M. Peyrin, β-amyloid induces a dying-back process and remote trans-synaptic alterations in a microfluidic-based reconstructed neuronal network, Acta Neuropathol. Commun. 2 (1) (2014) 145.
[55] M.J. Wilmer, C.P. Ng, H.L. Lanz, P. Vulto, L. Suter-Dick, R. Masereeuw, Kidney-on-a-chip technology for drug-induced nephrotoxicity screening, Trends Biotechnol. 34 (2) (2016) 156–170.
[56] L.A. Vernetti, N. Senutovitch, R. Boltz, R. DeBiasio, T. Ying Shun, A. Gough, D.L. Taylor, A human liver microphysiology platform for investigating physiology, drug safety, and disease models, Exp. Biol. Med. 241 (1) (2016) 101–114.
[57] S. Kim, A. Carlson, H. Cheng, S. Lee, J.-K. Park, Y. Huang, J.A. Rogers, Enhanced adhesion with pedestal-shaped elastomeric stamps for transfer printing, Appl. Phys. Lett. 100 (17) (2012).
[58] Y.-S. Torisawa, C.S. Spina, T. Mammoto, A. Mammoto, J.C. Weaver, T. Tat, J.J. Collins, D.E. Ingber, Bone marrow–on–a–chip replicates hematopoietic niche physiology in vitro, Nat. Methods 11 (6) (2014) 663.
[59] A. Grosberg, A.P. Nesmith, J.A. Goss, M.D. Brigham, M.L. McCain, K.K. Parker, Muscle on a chip: in vitro contractility assays for smooth and striated muscle, J. Pharmacol. Toxicol. Methods 65 (3) (2012) 126–135.
[60] D.R. Myers, Y. Sakurai, R. Tran, B. Ahn, E.T. Hardy, R. Mannino, A. Kita, M. Tsai, W.A. Lam, Endothelialized microfluidics for studying microvascular interactions in hematologic diseases, Journal of visualized experiments, JoVE 64 (2012).
[61] D. Huh, B.D. Matthews, A. Mammoto, M. Montoya-Zavala, H.Y. Hsin, D.E. Ingber, Reconstituting organ-level lung functions on a chip, Science 328 (5986) (2010) 1662–1668.
[62] K. Ronaldson-Bouchard, G. Vunjak-Novakovic, Organs-on-a-chip: a fast track for engineered human tissues in drug development, Cell Stem Cell 22 (3) (2018) 310–324.
[63] H. Shi, R.T. Kwok, J. Liu, B. Xing, B.Z. Tang, B. Liu, Real-time monitoring of cell apoptosis and drug screening using fluorescent light-up probe with aggregation-induced emission characteristics, J. Am. Chem. Soc. 134 (43) (2012) 17972–17981.
[64] D. Kim, S. Finkenstaedt-Quinn, K.R. Hurley, J.T. Buchman, C.L. Haynes, On-chip evaluation of platelet adhesion and aggregation upon exposure to mesoporous silica nanoparticles, Analyst 139 (5) (2014) 906–913.
[65] P.P. Laissue, R.A. Alghamdi, P. Tomancak, E.G. Reynaud, H.J.N.M. Shroff, Assessing phototoxicity in live fluorescence imaging, Nat. Methods 14 (7) (2017) 657.
[66] Y.I. Wang, H.E. Abaci, M.L. Shuler, Microfluidic blood–brain barrier model provides in vivo-like barrier properties for drug permeability screening, Biotechnol. Bioeng. 114 (1) (2017) 184–194.
[67] A. Weltin, K. Slotwinski, J. Kieninger, I. Moser, G. Jobst, M. Wego, R. Ehret, G.A. Urban, Cell culture monitoring for drug screening and cancer research: a transparent, microfluidic, multi-sensor microsystem, Lab on A Chip 14 (1) (2014) 138–146.
[68] S.R. Caliari, J.A. Burdick, A practical guide to hydrogels for cell culture, Nat Methods 13 (5) (2016) 405.
[69] M.S.R. Santoro, J.L. Shah, A.G. Walker, Mikos Poly (lactic acid) nanofibrous scaffolds for tissue engineering, Adv. Drug Deliv. Rev. 107 (2016) 206–212.
[70] M. Ravi, V. Paramesh, S. Kaviya, E. Anuradha, F.D. Solomon, 3D cell culture systems: advantages and Applications, J. Cell Physiol. 230 (1) (2015) 16–26.
[71] H. Cui, W. Zhu, M. Nowicki, X. Zhou, A. Khademhosseini, L.G. Zhang, Hierarchical fabrication of engineered vascularized bone biphasic constructs via dual 3D bioprinting: integrating regional bioactive factors into architectural design, Adv. Healthc. Mater. 5 (17) (2016) 2174–2181.
[72] H. Cui, W. Zhu, B. Holmes, L.G. Zhang, Biologically inspired smart release system based on 3D bioprinted perfused scaffold for vascularized tissue regeneration, Adv. Sci. (Weinh) 3 (8) (2016) 1600058.
[73] H. Cui, M. Nowicki, J.P. Fisher, L.G. Zhang, 3D bioprinting for organ regeneration, Adv. Healthc. Mater. 6 (1) (2017).
[74] S.-J. Lee, T. Esworthy, S. Stake, S. Miao, Y.Y. Zuo, B.T. Harris, L.G. Zhang, Advances in 3D bioprinting for neural tissue engineering, Adv. Biosyst. 2 (4) (2018).
[75] W. Zhu, T. Ye, S.J. Lee, H. Cui, S. Miao, X. Zhou, D. Shuai, L.G. Zhang, Enhanced neural stem cell functions in conductive annealed carbon nanofibrous scaffolds with electrical stimulation, Nanomedicine (2017).
[76] D.N. Heo, N. Acquah, J. Kim, S.J. Lee, N.J. Castro, L.G. Zhang, Directly induced neural differentiation of human adipose-derived stem cells using three-dimensional culture system of conductive microwell with electrical stimulation, Tissue Eng. Part A 24 (7–8) (2018) 537–545.
[77] S. Miao, N. Castro, M. Nowicki, L. Xia, H. Cui, X. Zhou, W. Zhu, S.J. Lee, K. Sarkar, G. Vozzi, Y. Tabata, J. Fisher, L.G. Zhang, 4D printing of polymeric materials for tissue and organ regeneration, Mater. Today (Kidlington) 20 (10) (2017) 577–591.
[78] A.S. Gladman, E.A. Matsumoto, R.G. Nuzzo, L. Mahadevan, J.A. Lewis, Biomimetic 4D printing, Nat. Mater. 15 (4) (2016) 413–418.
[79] B. Gao, Q. Yang, X. Zhao, G. Jin, Y. Ma, F. Xu, 4D Bioprinting for biomedical applications, Trends Biotechnol. 34 (9) (2016) 746–756.
[80] G. Villar, A.D. Graham, H. Bayley, A tissue-like printed material, Science 340 (6128) (2013) 48–52.

[81] G. Villar, A.J. Heron, H. Bayley, Formation of droplet networks that function in aqueous environments, Nat. Nanotechnol. 6 (12) (2011) 803–808.
[82] X.H. Qin, X. Wang, M. Rottmar, B.J. Nelson, K. Maniura-Weber, Near-infrared light-sensitive polyvinyl alcohol hydrogel photoresist for spatiotemporal control of cell-instructive 3D microenvironments, Adv. Mater. 30 (10) (2018) 1705564.
[83] S. Miao, H. Cui, M. Nowicki, S.J. Lee, J. Almeida, X. Zhou, W. Zhu, X. Yao, F. Masood, M.W. Plesniak, M. Mohiuddin, L.G. Zhang, Photolithographic-stereolithographic-tandem fabrication of 4D smart scaffolds for improved stem cell cardiomyogenic differentiation, Biofabrication 10 (3) (2018) 035007.
[84] S. Miao, H. Cui, M. Nowicki, L. Xia, X. Zhou, S.-J. Lee, W. Zhu, K. Sarkar, Z. Zhang, L.G. Zhang, Stereolithographic 4D bioprinting of multiresponsive architectures for neural engineering, Adv. Biosyst. 2 (9) (2018), https://doi.org/10.1002/adbi.201800101.
[85] S. Miao, W. Zhu, N.J. Castro, M. Nowicki, X. Zhou, H. Cui, J.P. Fisher, L.G. Zhang, 4D printing smart biomedical scaffolds with novel soybean oil epoxidized acrylate, Sci. Rep. 6 (2016) 27226.
[86] K. Qiu, Z. Zhao, G. Haghiashtiani, S.Z. Guo, M. He, R. Su, Z. Zhu, D.B. Bhuiyan, P. Murugan, F. Meng, 3D printed organ models with physical properties of tissue and integrated sensors, Adv. Mater. Technol. 3 (3) (2018) 1700235.
[87] E. Trampe, K. Koren, A.R. Akkineni, C. Senwitz, F. Krujatz, A. Lode, M. Gelinsky, M. Kühl, Functionalized bioink with optical sensor nanoparticles for O2 imaging in 3D-bioprinted constructs, Adv. Funct. Mater. 1804411 (2018).
[88] J.U. Lind, T.A. Busbee, A.D. Valentine, F.S. Pasqualini, H. Yuan, M. Yadid, S.-J. Park, A. Kotikian, A.P. Nesmith, P.H. Campbell, Instrumented cardiac microphysiological devices via multimaterial three-dimensional printing, Nat. Mater. 16 (3) (2017) 303.
[89] K. Nan, H. Luan, Z. Yan, X. Ning, Y. Wang, A. Wang, J. Wang, M. Han, M. Chang, K. Li, Engineered elastomer substrates for guided assembly of complex 3D mesostructures by spatially nonuniform compressive buckling, Adv. Funct. Mater. 27 (1) (2017) 1604281.
[90] Y. Liu, Z. Yan, Q. Lin, X. Guo, M. Han, K. Nan, K.C. Hwang, Y. Huang, Y. Zhang, J. A. Rogers, Guided formation of 3D helical mesostructures by mechanical buckling: analytical modeling and experimental validation, Adv. Funct. Mater. 26 (17) (2016) 2909–2918.
[91] Z. Fan, K.-C. Hwang, J.A. Rogers, Y. Huang, Y. Zhang, A double perturbation method of postbuckling analysis in 2D curved beams for assembly of 3D ribbon-shaped structures, J. Mech. Phys. Solids 111 (2018) 215–238.
[92] Y. Zhang, Z. Yan, K. Nan, D. Xiao, Y. Liu, H. Luan, H. Fu, X. Wang, Q. Yang, J. Wang, A mechanically driven form of Kirigami as a route to 3D mesostructures in micro/nanomembranes, Proc. Natl. Acad. Sci. U.S.A. 112 (38) (2015) 11757–11764.
[93] Z. Yan, F. Zhang, J. Wang, F. Liu, X. Guo, K. Nan, Q. Lin, M. Gao, D. Xiao, Y. Shi, Controlled mechanical buckling for origami-inspired construction of 3D microstructures in advanced materials, Adv. Funct. Mater. 26 (16) (2016) 2629–2639.
[94] Y. Shi, F. Zhang, K. Nan, X. Wang, J. Wang, Y. Zhang, Y. Zhang, H. Luan, K.-C. Hwang, Y. Huang, Plasticity-induced origami for assembly of three dimensional metallic structures guided by compressive buckling, Extreme Mech. Lett. 11 (2017) 105–110.
[95] Y.Y. Gao, H.Y. Cheng, Assembly of heterogeneous materials for biology and electronics: from bio-inspiration to bio-integration, J. Electron. Packag. 139 (2) (2017) 020801.
[96] S.Y. Yang, A. Carlson, H. Cheng, Q. Yu, N. Ahmed, J. Wu, S. Kim, M. Sitti, P.M. Ferreira, Y. Huang, J.A. Rogers, Elastomer surfaces with directionally dependent adhesion strength and their use in transfer printing with continuous roll-to-roll applications, Adv. Mater. 24 (16) (2012) 2117–2122.
[97] A. Carlson, A.M. Bowen, Y. Huang, R.G. Nuzzo, J.A. Rogers, Transfer printing techniques for materials assembly and micro/nanodevice fabrication, Adv. Mater. 24 (39) (2012) 5284–5318.
[98] Z. Yan, F. Zhang, F. Liu, M. Han, D. Ou, Y. Liu, Q. Lin, X. Guo, H. Fu, Z. Xie, Mechanical assembly of complex, 3D mesostructures from releasable multilayers of advanced materials, Sci. Adv. 2 (9) (2016) e1601014.
[99] J.M. McCracken, S. Xu, A. Badea, K.I. Jang, Z. Yan, D.J. Wetzel, K. Nan, Q. Lin, M. Han, M.A. Anderson, Deterministic integration of biological and soft materials onto 3D microscale cellular frameworks, Adv. Biosyst. 1 (9) (2017) 1700068.
[100] J.W. Jeong, M.K. Kim, H. Cheng, W.H. Yeo, X. Huang, Y. Liu, Y. Zhang, Y. Huang, J.A. Rogers, Capacitive epidermal electronics for electrically safe, long-term electrophysiological measurements, Adv. Healthc. Mater. 3 (5) (2014) 642–648.
[101] W.H. Yeo, Y.S. Kim, J. Lee, A. Ameen, L. Shi, M. Li, S. Wang, R. Ma, S.H. Jin, Z. Kang, Multifunctional epidermal electronics printed directly onto the skin, Adv. Mater. 25 (20) (2013) 2773–2778.
[102] J.J. Norton, D.S. Lee, J.W. Lee, W. Lee, O. Kwon, P. Won, S.-Y. Jung, H. Cheng, J.-W. Jeong, A. Akce, Soft, curved electrode systems capable of integration on the auricle as a persistent brain-computer interface, Proc. Natl. Acad. Sci. U.S. A. (2015) 201424875.
[103] L. Tian, Y. Li, R.C. Webb, S. Krishnan, Z. Bian, J. Song, X. Ning, K. Crawford, J. Kurniawan, A. Bonifas, Flexible and stretchable 3ω sensors for thermal characterization of human skin, Adv. Funct. Mater. 27 (26) (2017) 1701282.
[104] R.C. Webb, R.M. Pielak, P. Bastien, J. Ayers, J. Niittynen, J. Kurniawan, M. Manco, A. Lin, N.H. Cho, V. Malyrchuk, Thermal transport characteristics of human skin measured in vivo using ultrathin conformal arrays of thermal sensors and actuators, PLoS One 10 (2) (2015) e0118131.
[105] C. Dagdeviren, Y. Shi, P. Joe, R. Ghaffari, G. Balooch, K. Usgaonkar, O. Gur, P.L. Tran, J.R. Crosby, M. Meyer, Conformal piezoelectric systems for clinical and experimental characterization of soft tissue biomechanics, Nat. Mater. 14 (7) (2015) 728–736.
[106] Y. Shi, C. Dagdeviren, J. Rogers, C. Gao, Y. Huang, An analytic model for skin modulus measurement via conformal piezoelectric systems, J. Appl. Mech. 82 (9) (2015) 091007.
[107] A. Koh, D. Kang, Y. Xue, S. Lee, R.M. Pielak, J. Kim, T. Hwang, S. Min, A. Banks, P. Bastien, A soft, wearable microfluidic device for the capture, storage, and colorimetric sensing of sweat, Sci. Transl. Med. 8 (366) (2016) 366ra165.
[108] W. Gao, S. Emaminejad, H.Y.Y. Nyein, S. Challa, K. Chen, A. Peck, H.M. Fahad, H. Ota, H. Shiraki, D. Kiriya, Fully integrated wearable sensor arrays for multiplexed in situ perspiration analysis, Nature 529 (7587) (2016) 509–514.
[109] Y. Chen, S. Lu, S. Zhang, Y. Li, Z. Qu, Y. Chen, B. Lu, X. Wang, X.J.S.A. Feng, Skin-like biosensor system via electrochemical channels for noninvasive blood glucose monitoring, Sci. Adv. 3 (12) (2017) e1701629.
[110] W. Gao, H.Y. Nyein, Z. Shahpar, H.M. Fahad, K. Chen, S. Emaminejad, Y. Gao, L.-C. Tai, H. Ota, E. Wu, Wearable microsensor array for multiplexed heavy metal monitoring of body fluids, ACS Sens. 1 (7) (2016) 866–874.
[111] S. Yao, A. Myers, A. Malhotra, F. Lin, A. Bozkurt, J.F. Muth, Y. Zhu, A wearable hydration sensor with conformal nanowire electrodes, Adv. Healthc. Mater. 6 (6) (2017) 1601159.
[112] H.Y.Y. Nyein, W. Gao, Z. Shahpar, S. Emaminejad, S. Challa, K. Chen, H.M. Fahad, L.-C. Tai, H. Ota, R.W. Davis, A wearable electrochemical platform for noninvasive simultaneous monitoring of Ca2+ and pH, ACS Nano 10 (7) (2016) 7216–7224.
[113] S.-W. Hwang, H. Tao, D.-H. Kim, H. Cheng, J.-K. Song, E. Rill, M.A. Brenckle, B. Panilaitis, S.M. Won, Y.-S. Kim, Y.M. Song, K.J. Yu, A. Ameen, R. Li, Y. Su, M. Yang, D.L. Kaplan, M.R. Zakin, M.J. Slepian, Y. Huang, F.G. Omenetto, J.A. Rogers, A physically transient form of silicon electronics, Science 337 (6102) (2012) 1640–1644.
[114] S.W. Hwang, G. Park, H. Cheng, J.K. Song, S.K. Kang, L. Yin, J.H. Kim, F.G. Omenetto, Y. Huang, K.M. Lee, J.A. Rogers, 25th anniversary article: materials for high-performance biodegradable semiconductor devices, Adv. Mater. 26 (13) (2014) 1992–2000.
[115] M. Irimia-Vladu, "Green" electronics: biodegradable and biocompatible materials and devices for sustainable future, Chem. Soc. Rev. 43 (2) (2014) 588–610.
[116] M. Irimia-Vladu, E.D. Glowacki, G. Voss, S. Bauer, N.S. Sariciftci, Green and biodegradable electronics, Mater. Today 15 (7–8) (2012) 340–346.
[117] M.J. Tan, C. Owh, P.L. Chee, A.K.K. Kyaw, D. Kai, X.J. Loh, Biodegradable electronics: cornerstone for sustainable electronics and transient applications, J. Mater. Chem. C 4 (24) (2016) 5531–5558.
[118] S.K. Kang, J. Koo, Y.K. Lee, J.A. Rogers, Advanced materials and devices for bioresorbable electronics, ACC Chem. Res. 51 (5) (2018) 988–998.
[119] H.Y. Cheng, N. Yi, Dissolvable tattoo sensors: from science fiction to a viable technology, Phys. Scr. 92 (1) (2017) 013001.
[120] H. Cheng, Inorganic dissolvable electronics: materials and devices for biomedicine and environment, J. Mater. Res. 31 (17) (2016) 2549–2570.
[121] K.K. Fu, Z.Y. Wang, J.Q. Dai, M. Carter, L.B. Hu, Transient electronics: materials and devices, Chem. Mater. 28 (11) (2016) 3527–3539.
[122] L. Yin, H.Y. Cheng, S.M. Mao, R. Haasch, Y.H. Liu, X. Xie, S.W. Hwang, H. Jain, S. K. Kang, Y.W. Su, R. Li, Y.G. Huang, J.A. Rogers, Dissolvable metals for transient electronics, Adv. Funct. Mater. 24 (5) (2014) 645–658.
[123] Y. Zheng, X. Gu, F. Witte, Biodegradable metals, Mater. Sci. Eng. R: Rep. 77 (2014) 1–34.
[124] S.K. Kang, G. Park, K. Kim, S.W. Hwang, H. Cheng, J. Shin, S. Chung, M. Kim, L. Yin, J.C. Lee, K.M. Lee, J.A. Rogers, Dissolution chemistry and biocompatibility of silicon- and germanium-based semiconductors for transient electronics, ACS Appl. Mater. Interfaces 7 (17) (2015) 9297–9305.
[125] C. Dagdeviren, S.W. Hwang, Y. Su, S. Kim, H. Cheng, O. Gur, R. Haney, F.G. Omenetto, Y. Huang, J.A. Rogers, Transient, biocompatible electronics and energy harvesters based on ZnO, Small 9 (20) (2013) 3398–3404.
[126] S.H. Jin, S.-K. Kang, I.-T. Cho, S.Y. Han, H.U. Chung, D.J. Lee, J. Shin, G.W. Baek, T.-I. Kim, J.-H. Lee, Water-soluble thin film transistors and circuits based on amorphous indium–gallium–zinc oxide, ACS Appl. Mater. Interfaces 7 (15) (2015) 8268–8274.
[127] S.-K. Kang, S.-W. Hwang, H. Cheng, S. Yu, B.H. Kim, J.-H. Kim, Y. Huang, J.A. Rogers, Dissolution behaviors and applications of silicon oxides and nitrides in transient electronics, Adv. Funct. Mater. 24 (28) (2014) 4427–4434.
[128] S.W. Hwang, J.K. Song, X. Huang, H. Cheng, S.K. Kang, B.H. Kim, J.H. Kim, S. Yu, Y. Huang, J.A. Rogers, High-performance biodegradable/transient electronics on biodegradable polymers, Adv. Mater. 26 (23) (2014) 3905–3911.
[129] H.Y. Tian, Z.H. Tang, X.L. Zhuang, X.S. Chen, X.B. Jing, Biodegradable synthetic polymers: preparation, functionalization and biomedical application, Prog. Polym. Sci. 37 (2) (2012) 237–280.
[130] M.A. Brenckle, H. Cheng, S. Hwang, H. Tao, M. Paquette, D.L. Kaplan, J.A. Rogers, Y. Huang, F.G. Omenetto, Modulated degradation of transient electronic devices through multilayer silk fibroin pockets, ACS Appl. Mater. Interfaces 7 (36) (2015) 19870–19875.
[131] Y.J. Kim, S.E. Chun, J. Whitacre, C.J. Bettinger, Self-deployable current sources fabricated from edible materials, J. Mater. Chem. B 1 (31) (2013) 3781–3788.
[132] X. Huang, Y. Liu, S.W. Hwang, S.K. Kang, D. Patnaik, J.F. Cortes, J.A. Rogers, Biodegradable materials for multilayer transient printed circuit boards, Adv. Mater. 26 (43) (2014) 7371–7377.

[133] N. Yi, Z. Cheng, L. Yang, G. Edelman, C. Xue, Y. Ma, H. Zhu, H. Cheng, Fully water-soluble, high-performance transient sensors on a versatile galactomannan substrate derived from the endosperm, ACS Appl. Mater. Interfaces (2018).
[134] D.H. Kim, N. Lu, R. Ma, Y.S. Kim, R.H. Kim, S. Wang, J. Wu, S.M. Won, H. Tao, A. Islam, K.J. Yu, T.I. Kim, R. Chowdhury, M. Ying, L. Xu, M. Li, H.J. Chung, H. Keum, M. McCormick, P. Liu, Y.W. Zhang, F.G. Omenetto, Y. Huang, T. Coleman, J.A. Rogers, Epidermal electronics, Science 333 (6044) (2011) 838–843.
[135] C. Wang, C. Wang, Z. Huang, S. Xu, Materials and Structures toward Soft Electronics, Adv. Mater. 30 (50) (2018) 1801368.
[136] S.W. Hwang, C.H. Lee, H. Cheng, J.W. Jeong, S.K. Kang, J.H. Kim, J. Shin, J. Yang, Z. Liu, G.A. Ameer, Y. Huang, J.A. Rogers, Biodegradable elastomers and silicon nanomembranes/nanoribbons for stretchable, transient electronics, and biosensors, Nano Lett 15 (5) (2015) 2801–2808.
[137] K.J. Yu, D. Kuzum, S.W. Hwang, B.H. Kim, H. Juul, N.H. Kim, S.M. Won, K. Chiang, M. Trumpis, A.G. Richardson, H. Cheng, H. Fang, M. Thomson, H. Bink, D. Talos, K.J. Seo, H.N. Lee, S.K. Kang, J.H. Kim, J.Y. Lee, Y. Huang, F.E. Jensen, M. A. Dichter, T.H. Lucas, J. Viventi, B. Litt, J.A. Rogers, Bioresorbable silicon electronics for transient spatiotemporal mapping of electrical activity from the cerebral cortex, Nat. Mater. 15 (7) (2016) 782–791.
[138] S.K. Kang, R.K. Murphy, S.W. Hwang, S.M. Lee, D.V. Harburg, N.A. Krueger, J. Shin, P. Gamble, H. Cheng, S. Yu, Z. Liu, J.G. McCall, M. Stephen, H. Ying, J. Kim, G. Park, R.C. Webb, C.H. Lee, S. Chung, D.S. Wie, A.D. Gujar, B. Vemulapalli, A. H. Kim, K.M. Lee, J. Cheng, Y. Huang, S.H. Lee, P.V. Braun, W.Z. Ray, J.A. Rogers, Bioresorbable silicon electronic sensors for the brain, Nature 530 (7588) (2016) 71–76.
[139] S. Yang, Y.C. Chen, L. Nicolini, P. Pasupathy, J. Sacks, B. Su, R. Yang, D. Sanchez, Y.F. Chang, P. Wang, Cut-and-paste manufacture of multiparametric epidermal sensor systems, Adv. Mater. 27 (41) (2015) 6423–6430.
[140] Z. Huang, Y. Hao, Y. Li, H. Hu, C. Wang, A. Nomoto, T. Pan, Y. Gu, Y. Chen, T. Zhang, Three-dimensional integrated stretchable electronics, Nat. Electron. 1 (8) (2018) 473.
[141] B. Sun, R.N. McCay, S. Goswami, Y. Xu, C. Zhang, Y. Ling, J. Lin, Z. Yan, Gas-permeable, multifunctional on-skin electronics based on laser-induced porous graphene and sugar-templated elastomer sponges, Adv. Mater. 1804327 (2018).
[142] Y. Cao, G. Zhang, Y. Zhang, M. Yue, Y. Chen, S. Cai, T. Xie, X. Feng, Direct fabrication of stretchable electronics on a polymer substrate with process-integrated programmable rigidity, Adv. Funct. Mater. 1804604 (2018).
[143] H. Cheng, J. Wu, M. Li, D.H. Kim, Y.S. Kim, Y. Huang, Z. Kang, K.C. Hwang, J.A. Rogers, An analytical model of strain isolation for stretchable and flexible electronics, Appl. Phys. Lett. 98 (6) (2011) 061902.
[144] X. Yu, W. Shou, B.K. Mahajan, X. Huang, H. Pan, Materials, processes, and facile manufacturing for bioresorbable electronics: a review, Adv. Mater. 30 (28) (2018) e1707624.
[145] S.R. Gutbrod, M.S. Sulkin, J.A. Rogers, I.R. Efimov, Patient-specific flexible and stretchable devices for cardiac diagnostics and therapy, Prog. Biophys. Mol. Biol. 115 (2–3) (2014) 244–251.
[146] L. Xu, S.R. Gutbrod, A.P. Bonifas, Y. Su, M.S. Sulkin, N. Lu, H.-J. Chung, K.-I. Jang, Z. Liu, M. Ying, others, 3D multifunctional integumentary membranes for spatiotemporal cardiac measurements and stimulation across the entire epicardium, Nat. Commun. 5 (2014).
[147] L. Xu, S.R. Gutbrod, Y. Ma, A. Petrossians, Y. Liu, R.C. Webb, J.A. Fan, Z. Yang, R. Xu, J.J. Whalen III, Materials and fractal designs for 3D multifunctional integumentary membranes with capabilities in cardiac electrotherapy, Adv. Mater. 27 (10) (2015) 1731–1737.
[148] C. Dagdeviren, B.D. Yang, Y. Su, P.L. Tran, P. Joe, E. Anderson, J. Xia, V. Doraiswamy, B. Dehdashti, X. Feng, Conformal piezoelectric energy harvesting and storage from motions of the heart, lung, and diaphragm, Proc. Natl. Acad. Sci. U.S.A. 111 (5) (2014) 1927–1932.
[149] H. Wieneke, S. Rickers, J. Velleuer, G. Bruck, Z. Bai, C. Kocks, P.-A. Grandjean, T. Lenihan, P. Jung, R. Erbel, Leadless pacing using induction technology: impact of pulse shape and geometric factors on pacing efficiency, Europace 15 (3) (2012) 453–459.
[150] M. Madhavan, S.K. Mulpuru, C.J. McLeod, Y.-M. Cha, P.A. Friedman, Advances and future directions in cardiac pacemakers: part 2 of a 2-part series, J. Am. Coll. Cardiol. 69 (2) (2017) 211–235.
[151] G. Bozzuto, A. Molinari, Liposomes as nanomedical devices, Int. J. Nanomed. 10 (2015) 975.
[152] W. Alshaer, H. Hillaireau, J. Vergnaud, S. Ismail, E. Fattal, Functionalizing liposomes with anti-CD44 aptamer for selective targeting of cancer cells, Bioconjug. Chem. 26 (7) (2014) 1307–1313.
[153] E.M. Ahmed, Hydrogel: preparation, characterization, and applications: a review, J. Adv. Res. 6 (2) (2015) 105–121.
[154] P. Kesharwani, K. Jain, N.K. Jain, Dendrimer as nanocarrier for drug delivery, Prog. Polym. Sci. 39 (2) (2014) 268–307.
[155] H. Wang, Q. Huang, H. Chang, J. Xiao, Y. Cheng, Stimuli-responsive dendrimers in drug delivery, Biomater. Sci. 4 (3) (2016) 375–390.
[156] S.K. Sahoo, R. Misra, S. Parveen, Nanoparticles: a boon to drug delivery, therapeutics, diagnostics and imaging, Nanomedicine in Cancer, Pan Stanford (2017) 73–124.
[157] K. Yang, L. Feng, Z. Liu, Stimuli responsive drug delivery systems based on nano-graphene for cancer therapy, Adv. Drug Deliv. Rev. 105 (2016) 228–241.
[158] J. Liu, Y. Huang, A. Kumar, A. Tan, S. Jin, A. Mozhi, X.-J. Liang, pH-sensitive nano-systems for drug delivery in cancer therapy, Biotechnol. Adv. 32 (4) (2014) 693–710.
[159] V.P. Torchilin, Multifunctional, stimuli-sensitive nanoparticulate systems for drug delivery, Nat. Rev. Drug Discov. 13 (11) (2014) 813.
[160] K.-J. Chen, E.-Y. Chaung, S.-P. Wey, K.-J. Lin, F. Cheng, C.-C. Lin, H.-L. Liu, H.-W. Tseng, C.-P. Liu, M.-C. Wei, Hyperthermia-mediated local drug delivery by a bubble-generating liposomal system for tumor-specific chemotherapy, ACS Nano 8 (5) (2014) 5105–5115.
[161] B.R. Goldenbogen, N. Brodersen, A. Gramatica, M. Loew, J.R. Liebscher, A. Herrmann, H. Egger, B. Budde, A. Arbuzova, Reduction-sensitive liposomes from a multifunctional lipid conjugate and natural phospholipids: reduction and release kinetics and cellular uptake, Langmuir 27 (17) (2011) 10820–10829.
[162] D. Lee, K. Choe, Y. Jeong, J. Yoo, S.M. Lee, J.-H. Park, P. Kim, Y.-C. Kim, Establishment of a controlled insulin delivery system using a glucose-responsive double-layered nanogel, RSC Adv. 5 (19) (2015) 14482–14491.
[163] B.P. Timko, T. Dvir, D.S. Kohane, Remotely triggerable drug delivery systems, Adv. Mater. 22 (44) (2010) 4925–4943.
[164] M.-C. Chen, Z.-W. Lin, M.-H. Ling, Near-infrared light-activatable microneedle system for treating superficial tumors by combination of chemotherapy and photothermal therapy, ACS Nano 10 (1) (2015) 93–101.
[165] J. Di, S. Yao, Y. Ye, Z. Cui, J. Yu, T.K. Ghosh, Y. Zhu, Z. Gu, Stretch-triggered drug delivery from wearable elastomer films containing therapeutic depots, ACS Nano 9 (9) (2015) 9407–9415.
[166] J.L. Paris, M.V. Cabañas, M. Manzano, M. Vallet-Regí, Polymer-grafted mesoporous silica nanoparticles as ultrasound-responsive drug carriers, ACS Nano 9 (11) (2015) 11023–11033.
[167] Y. Brudno, D.J. Mooney, On-demand drug delivery from local depots, J. Control. Release 219 (2015) 8–17.
[168] K. van der Maaden, W. Jiskoot, J. Bouwstra, Microneedle technologies for (trans) dermal drug and vaccine delivery, J. Control. Release 161 (2) (2012) 645–655.
[169] Y. Zhang, J. Yu, J. Wang, N.J. Hanne, Z. Cui, C. Qian, C. Wang, H. Xin, J.H. Cole, C. M. Gallippi, Thrombin-responsive transcutaneous patch for auto-anticoagulant regulation, Adv. Mater. 29 (4) (2017) 1604043.
[170] J. Yu, C. Qian, Y. Zhang, Z. Cui, Y. Zhu, Q. Shen, F.S. Ligler, J.B. Buse, Z. Gu, Hypoxia and H2O2 dual-sensitive vesicles for enhanced glucose-responsive insulin delivery, Nano Lett. 17 (2) (2017) 733–739.
[171] M.R. Prausnitz, S. Mitragotri, R. Langer, Current status and future potential of transdermal drug delivery, Nat. Rev. Drug Discov. 3 (2) (2004) 115.
[172] V. Mathur, Y. Satrawala, M.S. Rajput, Physical and chemical penetration enhancers in transdermal drug delivery system, Asian J. Pharm. 4 (3) (2014).
[173] A.F. Kydonieus, Treatise on Controlled Drug Delivery: Fundamentals-Optimization-Applications, Routledge, 2017.
[174] S. Ge, Y. Lin, H. Lu, Q. Li, J. He, B. Chen, C. Wu, Y. Xu, Percutaneous delivery of econazole using microemulsion as vehicle: formulation, evaluation and vesicle-skin interaction, Int. J. Pharm. 465 (1–2) (2014) 120–131.
[175] F. Lai, R. Pireddu, F. Corrias, A.M. Fadda, D. Valenti, E. Pini, C. Sinico, Nanosuspension improves tretinoin photostability and delivery to the skin, Int. J. Pharm. 458 (1) (2013) 104–109.
[176] J. Cázares-Delgadillo, A. Ganem-Rondero, V. Merino, Y.N. Kalia, Controlled transdermal iontophoresis for poly-pharmacotherapy: Simultaneous delivery of granisetron, metoclopramide and dexamethasone sodium phosphate in vitro and in vivo, Eur. J. Pharm. Sci. 85 (2016) 31–38.
[177] F. Teodorescu, G. Queniat, C. Foulon, M. Lecoeur, A. Barras, S. Boulahneche, M. S. Medjram, T. Hubert, A. Abderrahmani, R. Boukherroub, Transdermal skin patch based on reduced graphene oxide: a new approach for photothermal triggered permeation of ondansetron across porcine skin, J. Control. Release 245 (2017) 137–146.
[178] T.A. Pereira, D.N. Ramos, R.F. Lopez, Hydrogel increases localized transport regions and skin permeability during low frequency ultrasound treatment, Sci. Rep. 7 (2017) 44236.
[179] J. Kim, D. Son, M. Lee, C. Song, J.-K. Song, J.H. Koo, D.J. Lee, H.J. Shim, J.H. Kim, M. Lee, A wearable multiplexed silicon nonvolatile memory array using nanocrystal charge confinement, Sci. Adv. 2 (1) (2016) e1501101.
[180] M.K. Choi, O.K. Park, C. Choi, S. Qiao, R. Ghaffari, J. Kim, D.J. Lee, M. Kim, W. Hyun, S.J. Kim, Cephalopod-inspired miniaturized suction cups for smart medical skin, Adv. Healthc. Mater. 5 (1) (2016) 80–87.
[181] H. Lee, C. Song, Y.S. Hong, M.S. Kim, H.R. Cho, T. Kang, K. Shin, S.H. Choi, T. Hyeon, D.-H. Kim, Wearable/disposable sweat-based glucose monitoring device with multistage transdermal drug delivery module, Sci. Adv. 3 (3) (2017) e1601314.
[182] H. Lee, T.K. Choi, Y.B. Lee, H.R. Cho, R. Ghaffari, L. Wang, H.J. Choi, T.D. Chung, N. Lu, T. Hyeon, A graphene-based electrochemical device with thermoresponsive microneedles for diabetes monitoring and therapy, Nat. Nanotechnol. 11 (6) (2016) 566.
[183] D. Son, J. Lee, D.J. Lee, R. Ghaffari, S. Yun, S.J. Kim, J.E. Lee, H.R. Cho, S. Yoon, S. Yang, Bioresorbable electronic stent integrated with therapeutic nanoparticles for endovascular diseases, ACS Nano 9 (6) (2015) 5937–5946.
[184] J. Koo, M.R. MacEwan, S.-K. Kang, S.M. Won, M. Stephen, P. Gamble, Z. Xie, Y. Yan, Y.-Y. Chen, J. Shin, N. Birenbaum, S. Chung, S.B. Kim, J. Khalifeh, D.V. Harburg, K. Bean, M. Paskett, J. Kim, Z.S. Zohny, S.M. Lee, R. Zhang, K. Luo, B. Ji, A. Banks, H.M. Lee, Y. Huang, W.Z. Ray, J.A. Rogers, Wireless bioresorbable electronic system enables sustained nonpharmacological neuroregenerative therapy, Nat. Med. (2018).
[185] L. Tang, P. Thevenot, W. Hu, Surface chemistry influences implant biocompatibility, Curr. Top. Med. Chem. 8 (4) (2008) 270–280.
[186] T. Thamaraiselvi, S. Rajeswari, Biological evaluation of bioceramic materials-a review, Carbon 24 (31) (2004) 172.

[187] D.F. Williams, On the mechanisms of biocompatibility, Biomaterials 29 (20) (2008) 2941–2953.
[188] J.M. Morais, F. Papadimitrakopoulos, D.J. Burgess, Biomaterials/tissue interactions: possible solutions to overcome foreign body response, AAPS J. 12 (2) (2010) 188–196.
[189] F. Variola, J.B. Brunski, G. Orsini, P.T. de Oliveira, R. Wazen, A. Nanci, Nanoscale surface modifications of medically relevant metals: state-of-the art and perspectives, Nanoscale 3 (2) (2011) 335–353.
[190] M.C. Bélanger, Y. Marois, Hemocompatibility, biocompatibility, inflammatory and in vivo studies of primary reference materials low-density polyethylene and polydimethylsiloxane: a review, J. Biomed. Mater. Res. 58 (5) (2001) 467–477.
[191] A.M. Pinto, I.C. Goncalves, F.D. Magalhaes, Graphene-based materials biocompatibility: a review, Colloids Surf. B Biointerfaces 111 (2013) 188–202.
[192] M.I. Baker, S.P. Walsh, Z. Schwartz, B.D. Boyan, A review of polyvinyl alcohol and its uses in cartilage and orthopedic applications, J. Biomed. Mater. Res. Part B Appl. Biomater. 100 (5) (2012) 1451–1457.
[193] A.T. Sidambe, Biocompatibility of advanced manufactured titanium implants-A review, Materials 7 (12) (2014) 8168–8188.
[194] I. 10993-1, Biological evaluation of medical devices–part 1: evaluation and testing, 2003.
[195] G. Kotzar, M. Freas, P. Abel, A. Fleischman, S. Roy, C. Zorman, J.M. Moran, J.J.B. Melzak, Evaluation of mems materials of construction for implantable medical devices, Biomaterials 23 (13) (2002) 2737–2750.
[196] K. Scholten, E. Meng, Materials for microfabricated implantable devices: a review, Lab Chip 15 (22) (2015) 4256–4272.
[197] S.W. Hwang, G. Park, C. Edwards, E.A. Corbin, S.K. Kang, H. Cheng, J.K. Song, J. H. Kim, S. Yu, J. Ng, J.E. Lee, J. Kim, C. Yee, B. Bhaduri, Y. Su, F.G. Omennetto, Y. Huang, R. Bashir, L. Goddard, G. Popescu, K.M. Lee, J.A. Rogers, Dissolution chemistry and biocompatibility of single-crystalline silicon nanomembranes and associated materials for transient electronics, ACS Nano 8 (6) (2014) 5843–5851.
[198] J.K. Chang, M.A.B. Emon, C.S. Li, Q. Yang, H.P. Chang, Z. Yang, C.I. Wu, M.T. Saif, J.A. Rogers, Cytotoxicity and in vitro degradation kinetics of foundry-compatible semiconductor nanomembranes and electronic microcomponents, ACS Nano (2018).
[199] P.P. Mueller, S. Arnold, M. Badar, D. Bormann, F.W. Bach, A. Drynda, A. Meyer-Lindenberg, H. Hauser, M. Peuster, Histological and molecular evaluation of iron as degradable medical implant material in a murine animal model, J. Biomed. Mater. Res. Part A 100 (11) (2012) 2881–2889.
[200] S.K. Kang, S.W. Hwang, S. Yu, J.H. Seo, E.A. Corbin, J. Shin, D.S. Wie, R. Bashir, Z. Ma, J.A. Rogers, Biodegradable thin metal foils and spin-on glass materials for transient electronics, Adv. Funct. Mater. 25 (12) (2015) 1789–1797.
[201] M. Irimia-Vladu, "Green" electronics: biodegradable and biocompatible materials and devices for sustainable future, Chem. Soc. Rev. 43 (2) (2014) 588–610.
[202] V.D. Prajapati, G.K. Jani, S.M. Khanda, Pullulan: an exopolysaccharide and its various applications, Carbohydr. Polym. 95 (1) (2013) 540–549.
[203] X. He, J. Zhang, W. Wang, W. Xuan, X. Wang, Q. Zhang, C.G. Smith, J. Luo, Transient resistive switching devices made from egg albumen dielectrics and dissolvable electrodes, ACS Appl. Mater. Interfaces 8 (17) (2016) 10954–10960.
[204] J.M. Anderson, A. Rodriguez, D.T. Chang, Foreign body reaction to biomaterials, Semin. Immunol. (2008) 86–100.
[205] H. Fu, K. Nan, P. Froeter, W. Huang, Y. Liu, Y. Wang, J. Wang, Z. Yan, H. Luan, X. Guo, Mechanically-guided deterministic assembly of 3D mesostructures assisted by residual stresses, Small 13 (24) (2017) 1700151.
[206] X. Guo, X. Wang, D. Ou, J. Ye, W. Pang, Y. Huang, J.A. Rogers, Y. Zhang, Controlled mechanical assembly of complex 3D mesostructures and strain sensors by tensile buckling, npj Flexible, Electronics 2 (1) (2018) 14.
[207] X. Ning, H. Wang, X. Yu, J.A. Soares, Z. Yan, K. Nan, G. Velarde, Y. Xue, R. Sun, Q. Dong, 3D tunable, multiscale, and multistable vibrational micro-platforms assembled by compressive buckling, Adv. Funct. Mater. 27 (14) (2017) 1605914.
[208] H. Fu, K. Nan, W. Bai, W. Huang, K. Bai, L. Lu, C. Zhou, Y. Liu, F. Liu, J. Wang, Morphable 3D mesostructures and microelectronic devices by multistable buckling mechanics, Nat. Mater. 17 (3) (2018) 268.
[209] W. Lee, Y. Liu, Y. Lee, B.K. Sharma, S.M. Shinde, S.D. Kim, K. Nan, Z. Yan, M. Han, Y. Huang, Two-dimensional materials in functional three-dimensional architectures with applications in photodetection and imaging, Nat. Commun. 9 (1) (2018) 1417.
[210] B.H. Kim, J. Lee, S.M. Won, Z. Xie, J.-K. Chang, Y. Yu, Y.K. Cho, H. Jang, J.Y. Jeong, Y. Lee, Three-dimensional silicon electronic systems fabricated by compressive buckling process, ACS Nano 12 (5) (2018) 4164–4171.
[211] X. Ning, X. Yu, H. Wang, R. Sun, R. Corman, H. Li, C.M. Lee, Y. Xue, A. Chempakasseril, Y. Yao, Mechanically active materials in three-dimensional mesostructures, Sci. Adv. 4 (9) (2018) eaat8313.
[212] K.-I. Jang, K. Li, H.U. Chung, S. Xu, H.N. Jung, Y. Yang, J.W. Kwak, H.H. Jung, J. Song, C. Yang, Self-assembled three dimensional network designs for soft electronics, Nat. Commun. 8 (2017) 15894.
[213] H. Cui, S. Miao, T. Esworthy, X. Zhou, S.-J. Lee, C. Liu, Z.-X. Yu, J.P. Fisher, M. Mohiuddin, L.G. Zhang, 3D bioprinting for cardiovascular regeneration and pharmacology, Adv. Drug Deliv. Rev. (2018).
[214] M. Caralt, J.S. Uzarski, S. Iacob, K.P. Obergfell, N. Berg, B.M. Bijonowski, K.M. Kiefer, H.H. Ward, A. Wandinger-Ness, W.M. Miller, Optimization and critical evaluation of decellularization strategies to develop renal extracellular matrix scaffolds as biological templates for organ engineering and transplantation, Am. J. Transpl. 15 (1) (2015) 64–75.
[215] E.A. Calle, T.H. Petersen, L.E. Niklason, Procedure for lung engineering, Journal of visualized experiments, JoVE 49 (2011).
[216] T.-Y. Lu, B. Lin, J. Kim, M. Sullivan, K. Tobita, G. Salama, L. Yang, Repopulation of decellularized mouse heart with human induced pluripotent stem cell-derived cardiovascular progenitor cells, Nat. Commun. 4 (2013) 2307.
[217] N. Momtahan, N. Poornejad, J.A. Struk, A.A. Castleton, B.J. Herrod, B.R. Vance, J.P. Eatough, B.L. Roeder, P.R. Reynolds, A.D. Cook, Automation of pressure control improves whole porcine heart decellularization, Tissue Eng. Part C Methods 21 (11) (2015) 1148–1161.
[218] J. Hülsmann, H. Aubin, A. Kranz, E. Godehardt, H. Munakata, H. Kamiya, M. Barth, A. Lichtenberg, P. Akhyari, A novel customizable modular bioreactor system for whole-heart cultivation under controlled 3D biomechanical stimulation, J. Artif. Organs 16 (3) (2013) 294–304.
[219] G.B. Wanna, J.H. Noble, M.L. Carlson, R.H. Gifford, M.S. Dietrich, D.S. Haynes, B.M. Dawant, R.F. Labadie, Impact of electrode design and surgical approach on scalar location and cochlear implant outcomes, Laryngoscope 124 (S6) (2014) S1–S7.
[220] S.J. Rebscher, A. Hetherington, B. Bonham, P. Wardrop, D. Whinney, P.A. Leake, Considerations for the design of future cochlear implant electrode arrays: electrode array stiffness, size and depth of insertion, J. Rehabil. Res. Dev. 45 (5) (2008) 731.
[221] J.L. Pinyon, S.F. Tadros, K.E. Froud, A.C. Wong, I.T. Tompson, E.N. Crawford, M. Ko, R. Morris, M. Klugmann, G.D. Housley, Close-field electroporation gene delivery using the cochlear implant electrode array enhances the bionic ear, Sci. Transl. Med. 6 (233) (2014) 233ra54.
[222] Y. Buganim, D.A. Faddah, R. Jaenisch, Mechanisms and models of somatic cell reprogramming, Nat. Rev. Genet. 14 (6) (2013) 427.
[223] J. Couzin-Frankel, Cancer Immunotherapy, American Association for the Advancement of Science, 2013.
[224] M. Tabebordbar, K. Zhu, J.K. Cheng, W.L. Chew, J.J. Widrick, W.X. Yan, C. Maesner, E.Y. Wu, R. Xiao, F.A.J.S. Ran, In vivo gene editing in dystrophic mouse muscle and muscle stem cells, 351 (6271) (2016) 407–411.
[225] W. Bai, T. Kuang, C. Chitrakar, R. Yang, S. Li, D. Zhu, L. Chang, Patchable micro/nanodevices interacting with skin, Biosens. Bioelectron. (2018).
[226] D. Gallego-Perez, D. Pal, S. Ghatak, V. Malkoc, N. Higuita-Castro, S. Gnyawali, L. Chang, W.-C. Liao, J. Shi, M. Sinha, Topical tissue nano-transfection mediates non-viral stroma reprogramming and rescue, Nat. Nanotechnol. 12 (10) (2017) 974.
[227] J.W. Jeong, W.H. Yeo, A. Akhtar, J.J. Norton, Y.J. Kwack, S. Li, S.Y. Jung, Y. Su, W. Lee, J. Xia, H. Cheng, Y. Huang, W.S. Choi, T. Bretl, J.A. Rogers, Materials and optimized designs for human-machine interfaces via epidermal electronics, Adv. Mater. 25 (47) (2013) 6839–6846.
[228] J.J.S. Norton, D.S. Lee, J.W. Lee, W. Lee, O. Kwon, P. Won, S.Y. Jung, H.Y. Cheng, J.W. Jeong, A. Akce, S. Umunna, I. Na, Y.H. Kwon, X.Q. Wang, Z.J. Liu, U. Paik, Y. G. Huang, T. Bretl, W.H. Yeo, J.A. Rogers, Soft, curved electrode systems capable of integration on the auricle as a persistent brain-computer interface, Proc. Natl. Acad. Sci. U.S.A. 112 (13) (2015) 3920–3925.
[229] S. Raspopovic, M. Capogrosso, F.M. Petrini, M. Bonizzato, J. Rigosa, G. Di Pino, J. Carpaneto, M. Controzzi, T. Boretius, E. Fernandez, Restoring natural sensory feedback in real-time bidirectional hand prostheses, Sci. Transl. Med. 6 (222) (2014) 222ra19.
[230] H.J. Witteveen, F. Luft, J.S. Rietman, P.H. Veltink, Stiffness feedback for myoelectric forearm prostheses using vibrotactile stimulation, IEEE Trans. Neural Syst. Rehabil. Eng. 22 (1) (2014) 53–61.
[231] C. Dietrich, K. Walter-Walsh, S. Preißler, G.O. Hofmann, O.W. Witte, W.H. Miltner, T. Weiss, Sensory feedback prosthesis reduces phantom limb pain: proof of a principle, Neurosci. Lett. 507 (2) (2012) 97–100.
[232] J. Gonzalez, H. Soma, M. Sekine, W. Yu, Psycho-physiological assessment of a prosthetic hand sensory feedback system based on an auditory display: a preliminary study, J. Neuroeng. Rehabil. 9 (1) (2012) 33.